

6-16-2011

Characterizing Cyclostationary Features of Digital Modulated Signals with Empirical Measurements Using Spectral Correlation Function

Mujun Song

Follow this and additional works at: <https://scholar.afit.edu/etd>

Part of the [Power and Energy Commons](#), and the [Signal Processing Commons](#)

Recommended Citation

Song, Mujun, "Characterizing Cyclostationary Features of Digital Modulated Signals with Empirical Measurements Using Spectral Correlation Function" (2011). *Theses and Dissertations*. 1429.
<https://scholar.afit.edu/etd/1429>

This Thesis is brought to you for free and open access by the Student Graduate Works at AFIT Scholar. It has been accepted for inclusion in Theses and Dissertations by an authorized administrator of AFIT Scholar. For more information, please contact richard.mansfield@afit.edu.



**CHARACTERIZING CYCLOSTATIONARY FEATURES OF DIGITAL
MODULATED SIGNALS WITH EMPIRICAL MEASUREMENTS USING
SPECTRAL CORRELATION FUNCTION**

THESIS

Mujun Song, Captain, ROKA

AFIT/GCE/ENG/11-09

**DEPARTMENT OF THE AIR FORCE
AIR UNIVERSITY**

AIR FORCE INSTITUTE OF TECHNOLOGY

Wright-Patterson Air Force Base, Ohio

APPROVED FOR PUBLIC RELEASE; DISTRIBUTION UNLIMITED

The views expressed in this thesis are those of the author and do not reflect the official policy or position of the United States Air Force, Department of Defense, or the U.S. Government. This material is declared a work of the U.S. Government and is not subject to copyright protection in the United States.

AFIT/GCE/ENG/11-09

**CHARACTERIZING CYCLOSTATIONARY FEATURES OF DIGITAL
MODULATED SIGNALS WITH EMPIRICAL MEASUREMENTS USING
SPECTRAL CORRELATION FUNCTION**

THESIS

Presented to the Faculty

Department of Electrical and Computer Engineering

Graduate School of Engineering and Management

Air Force Institute of Technology

Air University

Air Education and Training Command

In Partial Fulfillment of the Requirements for the

Degree of Master of Science

Mujun Song, BS

Captain, ROKA

June 2011

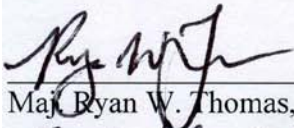
APPROVED FOR PUBLIC RELEASE; DISTRIBUTION UNLIMITED

**CHARACTERIZING CYCLOSTATIONARY FEATURES OF DIGITAL
MODULATED SIGNALS WITH EMPIRICAL MEASUREMENTS USING
SPECTRAL CORRELATION FUNCTION**

Mujun Song, BS

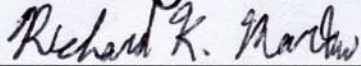
Captain, ROKA

Approved:



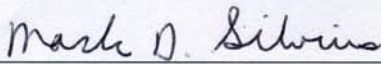
Maj. Ryan W. Thomas, PhD, USAF (Chairman)

20 May 2011
Date



Dr. Richard K. Martin, PhD (Member)

20 May 2011
Date



Maj. Mark D. Silvius, PhD, USAF (Member)

20 May 2011
Date

Abstract

Signal detection is widely used in many applications. Some examples include Cognitive Radio (CR) and military intelligence. CRs use signal detection to sense spectral occupancy. Without guaranteed signal detection, a CR cannot reliably perform its role. Similarly, signal detection is the first step for garnering an opponent's information.

Wireless signal detection can be performed using many different techniques. Some of the most popular include matched filters, energy detectors (which use measurements such as the Power Spectral Density (PSD) of the signal), and Cyclostationary Feature Detectors (CFD) [1]. Among these techniques, CFD can be viewed as a compromise technique, in that it theoretically has better low Signal-to-Noise Ratio (SNR) detection performance than energy detectors and less strict requirements than matched filters.

CFD uses the cyclostationarity of a signal to detect its presence. Signals that have cyclostationarity exhibit correlations between widely separated spectral components. Functions that describe this cyclostationarity include the Spectral Correlation Function (SCF). One advantage of cyclostationary approaches such as these is that Additive White Gaussian Noise (AWGN) is cancelled in these functions. This characteristic makes SCF outperform PSD under low SNR environments.

However, whereas the PSD has been well investigated through empirical experiments, the SCF features under real world noise have not been. In this effort, the SCF features of modulated signals under real world channel noise are first identified and

characterized using the concept of path loss. Second, the performance of the SCF under a low SNR environment with real world signals is examined with real world signals and noise. Third, the dependence between observation time of the SCF calculation and the SCF feature statistics are identified with real world signals. Lastly, reasons for discrepancies between the real-world and analytic / simulation based performance are suggested.

Acknowledgments

This work is dedicated to my heavenly Father, God, and my family. I would like to express my sincere appreciation to my faculty advisor, Maj. Ryan W. Thomas, for his guidance and support throughout the course of this thesis effort.

Mujun Song

Table of Contents

	Page
Abstract	iv
Acknowledgments.....	vi
Table of Contents	vii
List of Figures	ix
List of Tables	xi
I. Introduction	1
1.1 Background	1
1.2 Problem Statement / Goals.....	2
1.3 Scope	3
1.4 Approach	4
1.5 Organization.....	5
II. Literature Review	6
2.1 Chapter Overview	6
2.2 Spectral Correlation Function (SCF)	7
2.3 Detection Techniques.....	17
2.4 Channel Noise Analysis	24
2.5 Discussions.....	29
III. Methodology	33
3.1 Introduction	33
3.2 Problem Definition.....	33
3.3 System Boundaries.....	36
3.4 System Services.....	37

3.5	Workload.....	37
3.6	Performance Metrics	39
3.7	System Parameters	39
3.8	Factors	41
3.9	Evaluation Technique.....	46
3.10	Test bed.....	46
3.11	Design of Experiments (DOE).....	53
3.12	Analysis.....	54
3.13	Summary.....	54
IV.	Analysis and Results.....	55
4.1	Chapter Overview	55
4.2	Results	55
4.3	Summary	81
V.	Conclusions and Recommendations	82
5.1	Overview	82
5.2	Conclusions	82
5.3	Contributions.....	83
5.4	Future Work	84
	Appendix A : Simulink model	85
	Appendix B : Different computational approaches of SCF.....	87
	Bibliography	89
	Vita	94

List of Figures

	Page
Figure 1. Theoretical SCF magnitude surfaces for BPSK, QPSK, SQPSK with carrier frequency $f_0 = 3.3/T_0$ [15]	13
Figure 2. Theoretical Spectral correlation magnitude for 4-FSK signal with $\{(f_0 + f_m)T_0\} = \{5, 6, 7, 8\}$ [15]	15
Figure 3 . SCF and PSD of BPSK.....	16
Figure 4. Two approaches of Energy detection. [21].....	19
Figure 5. Implementation of a cyclostationary feature detection [20].....	23
Figure 6. Noise in the wireless channel [30].....	24
Figure 7. Multiplicative noise components in real world : Path loss, Shadowing, Multipath	26
Figure 8. SCF of BPSK under different SNR/observation time compared with PSD [7]	30
Figure 9. System Under Test (SUT)	36
Figure 10. Estimating the received signal power under $SNR < 0$ (dB)	44
Figure 11. Test bed for experiments	46
Figure 12. Simulink block model.....	49
Figure 13. Frequency offset in USRP2.....	50
Figure 14. dB offset in USRP2 and Spectrum analyzer.....	51
Figure 15. Anechoic chamber	57
Figure 16. Hallway.....	59
Figure 17. Auditorium	61

Figure 18. ANiMaL Lab	63
Figure 19. Hallway without LOS	66
Figure 20. In between buildings.....	68
Figure 21. Next to building without LOS	70
Figure 22. Parking lot	72
Figure 23. SCF vs. PSD with varying SNR and observation time	75
Figure 24. SCF of 2-FSK on different observation time	77
Figure 25. QQ Plot of AWGN and Real world noise	79
Figure 26. SCF Distribution of AWGN and Real world noise	80
Figure 27. Simulink block sets.....	85
Figure 28. SCFs of real 2-FSK, BPSK, and synthetic BPSK using different computational approaches.....	88

List of Tables

	Page
Table 1. Path Loss Exponents for different environment [32].....	28
Table 2. Statistical Properties of Time Smoothed and Instantaneous PSD/SCF [12]	30
Table 3. Location Factor	43
Table 4. Variance of SCF / PSD at each observation time in anechoic chamber	58
Table 5. Variance of SCF / PSD at each observation time at hallway.....	60
Table 6. Variance of SCF / PSD at each observation time at Auditorium.....	62
Table 7. Variance of SCF / PSD at each observation time at ANiMaL Lab	64
Table 8. Variance of SCF / PSD at each observation time at Hallway without LOS	67
Table 9. Variance of SCF / PSD at each observation time at between buildings	69
Table 10. Variance of SCF / PSD at each observation time next to building.....	71
Table 11. Variance of SCF / PSD at each observation time at Parking Lot	73
Table 12. Path loss exponents in each locations / path loss exponent differences to anechoic chamber / variance	73
Table 13. Variance ratios of theoretical and experimental $re\{\overline{S_{x+c}^\alpha(k)}\}$	78

CHARACTERIZING CYCLOSTATIONARY FEATURES OF DIGITAL MODULATED SIGNALS WITH EMPIRICAL MEASUREMENTS USING SPECTRAL CORRELATION FUNCTION

I. Introduction

1.1 Background

Signal detection is widely used in many applications. Some examples include cognitive radio and military intelligence. Cognitive radios (CRs) are radios that are “aware of [their] surroundings and adapt intelligently” [2]. The term “surroundings” most often refers to other users of spectrum. When performing Dynamic Spectrum Access (DSA), a cognitive radio acts as a secondary user that has to detect and identify other radio users in order to not interfere. To accomplish this, CRs use signal detection to sense spectral occupancy. Without guaranteed signal detection, a CR cannot reliably perform its role.

Similarly, signal detection also plays a key role in military intelligence. To know an opponent’s information in the battlefield is as critical as knowing an ally’s information. Signal detection is the first step for garnering an opponent’s information.

Wireless signal detection can be performed using many different techniques. Some of the most popular include matched filters, energy detectors (which use measurements such as the Power Spectral Density (PSD) of the signal), and Cyclostationary Feature Detectors (CFD) [1]. Each of these techniques has advantages and disadvantages in terms of theoretical and real world performance.

Among these techniques, CFD can be viewed as a compromise technique, in that it theoretically has better low Signal-to-Noise Ratio (SNR) detection performance than energy detectors and less strict requirements than matched filters. Therefore the CFD is regarded as a promising technique for signal detection.

CFD uses the cyclostationarity of a signal to detect its presence. Signals that have cyclostationarity exhibit correlations between widely separated spectral components. Functions that describe this cyclostationarity include the Spectral Correlation Function (SCF).

One advantage of cyclostationary approaches such as the SCF is that Additive White Gaussian Noise (AWGN) is cancelled in these functions. This is because there is no correlation between the noise spectrum and the signal spectrum. In contrast, other approaches such as energy detection are not robust to noise that under low SNR signals are hidden under noise. This characteristic makes SCF outperform PSD under low SNR environments.

1.2 Problem Statement / Goals

PSD has been well investigated, with “log-normal shadowing” often used as a representative model of how PSD works under real-world noise. However, SCF features under real world noise have not been as well investigated under empirical experiments. That is, how the SCF works under real world noise has not been studied.

The outperformance of the SCF under real world noise has not been shown under real-world conditions. Instead, it has been proven in analytic / simulation manner or with real experiments using AWGN (synthetic noise) as noise. But real world noise can be

different from AWGN, and there are other factors to consider such as path loss, shadowing, multipath fading, and interference [3].

In addition, under discrete, finite estimate of the cyclostationarity, there is dependence between its finite time parameter and SCF feature values, identified analytically in statistical view. It also has not been proven with real world signals.

Therefore, the goals of this research are

- To identify and characterize the SCF features of modulated signal under real world channel noise.
- To examine the performance of the SCF under low SNR environment with real world signal.
- To observe the correlation between finite time parameter of the SCF calculation and its feature values with real world signal

1.3 Scope

During this research, 2-Frequency Shift Keying (FSK) modulation is used with 20 KS/s symbol rate at 2.45 GHz band. The signal is generated from signal generator, Agilent E4438C, ESG Vector Signal Generator. Universal Software Radio Peripheral 2 (USRP2), which is a Software Defined Radio (SDR), is used as a receiver. The receiver samples the signal at 800 KS/s. Because of USRP2 hardware limitation (will be discussed later), only positive frequency band of received signal is considered. The receiver and the transmitter are static while taking measurements. Thus, Doppler effects are not

considered in the research. To get the cyclostationary features of the modulated signal, SCF is used, and implemented in Simulink.

Analysis of path loss is based on the “log-normal shadowing” model for both indoor and outdoor experiments. Any other detailed path loss models are not considered. Curve fitting for measured data is performed using Least Squares curve fitting method which minimizes deviation from all data points.

1.4 Approach

According to the goals stated above, experimental approach was determined.

To identify and characterize the SCF features of modulated signal under real world channel noise, we measure the path loss exponent of SCF and compare it to the path loss exponent of PSD. Experiments for path loss are performed by varying locations and distances. Resultant path loss for each location is analyzed in terms of path loss exponents and variance of feature magnitudes.

To examine the performance of SCF under low SNR environment with real world signals, we obtain SCF features under different SNR levels with varying observation times. SNR levels range from -40dB to 20dB to examine its performance under low and high SNR environments. In addition, observation time is also varied to identify its effect on SNR performance.

To observe the correlation between finite time parameter of SCF calculation and its feature values with real world signal, we investigate the dependence between observation time of SCF and variance of SCF feature values. The result will be compared to analytic result.

1.5 Organization

The rest of this thesis is organized as follows: Chapter 2 covers a literature review of related work. An overview of cyclostationarity and SCF and its attributes are given with theoretical formula. Its applications and cyclostationary features of modulated signals are also discussed. After that, channel noise effects in the real world are introduced. Lastly, recent research on SCF, especially on SCF features under noise and its statistical characters, is introduced. Chapter 3 talks about methodology of how to define parameters of experiments and how to set up the physical experiment test bed including the transmitter, receiver and SCF analyzer and environment which affects the level of noise. SCF features of real world signals are compared with PSD features and theoretical SCF features in chapter 4. Chapter 5 restates the results of this research and explains contributions of this work.

II. Literature Review

2.1 Chapter Overview

Most signals of interest for detection are uniquely modulated. Examples include the communications signals that secondary user radios try to detect in dynamic spectrum access schemes and radar waveforms that are intercepted in the military. One aspect of these modulated signals that can be used for signal detection is a cyclostationary feature. One tool to detect cyclostationarity is Spectral Correlation Function (SCF), which can be thought of as a more generalized form of Power Spectral Density (PSD). The SCF is used in signal processing areas such as signal detection, parameter estimation, and signal classification [4] [5]. The reason why it is used is that it is robust to noise and has different unique feature sets for different modulations.

Signals are transmitted using spectrum as a medium in wireless communication. However spectrum is not a “clean” medium, which means that it carries not only the signal of interest but also noise and interference. Also, there can be distorting effects such as shadowing and multipath. All of these make it difficult to detect signals. The SCF theoretically has better performance in noisy environments than PSD [6]; white Gaussian noise shows little spectral correlation within the noise, and modulated signal has its own spectral correlation feature within itself, which makes SCF more outstanding. However, there can still exist spectral correlation between the noise and the signal due to the limited sample sizes, which is called cross-SCF [4]. The effect of cross-SCF can be bigger if the noise is not truly white, making feature of the signal less visible because it is hidden by spectral correlation within the noise itself and between noise and the signal.

The remainder of this chapter is organized as follows: Section 2 will discuss what the cyclostationarity and SCF are, including properties of SCF and SCF feature of Frequency Shift Keying (FSK) modulated signal. Section 3 will introduce several detection techniques and provide some reasons why cyclostationary feature detection is better than other detection techniques. Noise components such as fading and interference, which hinder transmitting signal correctly, are introduced and some of them, such as AWGN and fading, are dealt with through looking into what have been done to understand how SCF is affected by them.

2.2 Spectral Correlation Function (SCF)

Cyclostationary features of signals are measured using SCF. That is, SCF is used to show cyclostationarity of signals. Therefore, before the SCF is investigated, cyclostationarity is introduced first.

2.2.1 Cyclostationarity

Stationary processes are processes whose mean and autocorrelation do not change as time changes. Cyclostationary processes, which have the property of “cyclostationarity,” are processes whose statistical parameters, mean and autocorrelation, show periodicity [8]. That is, its mean and autocorrelation change with periodicity as time varies. This periodicity is called second-order periodicity. Many stochastic processes generated by technical processes exhibit cyclostationarity. Examples include most modulated communication signals and vibration noise produced by rotating machines [8].

Cyclostationarity is described mathematically as [9] :

$$\begin{aligned}
M_x(t+T_0) &= M_x(t) \\
R_x(t+T_0, \tau) &= R_x(t, \tau)
\end{aligned} \tag{1}$$

where $R_x(t, \tau) \triangleq E\{x(t+\tau/2)x^*(t-\tau/2)\}$ [6], $M_x(t)$ is mean of process $x(t)$ at time t and $R_x(t, \tau)$ is autocorrelation of process $x(t)$ with time difference τ and $E\{\cdot\}$ denotes the mathematical expectation operation. T_0 is a period [9].

2.2.2 Definition of Spectral Correlation Function (SCF)

The SCF represents how much the spectral components of a process are correlated with other spectral components of the process. The SCF can be derived from Cyclic Autocorrelation Function (CAF). Before looking into SCF, we define the CAF to understand the concept of cycle frequency.

As previously described, a cyclostationary process exhibits periodicity in its autocorrelation. If the autocorrelation of a process is periodic with T_0 , it indicates that the autocorrelation has its own frequency, called the *cycle frequency* (denoted by α), which can be described as $\alpha = m/T_0$ where m is integer. Since it is periodic with frequency α , it can be described in Fourier series [9].

$$R_x(t, \tau) = \sum_{\alpha} R_x^{\alpha}(\tau) e^{i2\pi\alpha t} \tag{2}$$

where $R_x^{\alpha}(\tau)$ is the CAF of process $x(t)$ with cycle frequency α , which is also the Fourier coefficients of the autocorrelation of process $x(t)$. Thus, the Fourier coefficients can be expressed as

$$R_x^\alpha(\tau) \triangleq \lim_{T \rightarrow \infty} \frac{1}{T} \int_{-T/2}^{T/2} R_x(t, \tau) e^{-i2\pi\alpha t} dt \quad (3)$$

for more than one periodicity [4][5]. In short, the CAF, $R_x^\alpha(\tau)$, can be said to indicate the magnitude of the autocorrelation with τ of $x(t)$ at a component cycle frequency α . In addition, an interesting thing is that if the cyclic autocorrelation is not periodic but constant (that is, $\alpha = 0$) it is equal to simple autocorrelation, which means that cyclic autocorrelation includes autocorrelation.

According to the Wiener relation, the Fourier transform of autocorrelation is identical to PSD. The Wiener relation can extend to cyclic autocorrelation, resulting in cyclic Wiener relation which embraces the $\alpha \neq 0$ cases [10]. According to the cyclic Wiener relation, the Fourier transform of the CAF is equal to SCF, expressed as [11]

$$S_x^\alpha(f) = \int_{-\infty}^{\infty} R_x^\alpha(\tau) e^{-i2\pi f \tau} d\tau \quad (4)$$

Another derivation of SCF is from spectral cross-correlation. With special two complex-valued $\alpha/2$ frequency shifted version of process $x(t)$,

$$\begin{aligned} u(t) &\triangleq x(t) e^{-i2\pi(\frac{\alpha}{2})t} \\ v(t) &\triangleq x(t) e^{-i2\pi(-\frac{\alpha}{2})t} \end{aligned} \quad (5)$$

Cross-spectrum of the two process $u(t)$, $v(t)$ is defined to be spectral correlation function of $x(t)$ as below. It is also called as *cyclic spectrum* [11].

$$S_{uv}(f) \triangleq S_x^\alpha(f) \quad (6)$$

That is, $S_x^\alpha(f)$ is the correlation of the two spectral components of $x(t)$, at frequencies $f + \alpha/2$ and $f - \alpha/2$.

Considering a practical situation, in which the signal has finite-samples and is time-variant, the T -windowed normalized time-variant finite-time Fourier transform is defined as [7]

$$X_T(t, f) \triangleq \frac{1}{\sqrt{T}} \int_{t-T/2}^{t+T/2} x(u) e^{-i2\pi fu} du \quad (7)$$

Therefore, T -windowed time-variant finite-time Fourier transforms of $u(t)$ and $v(t)$ are $U_T(t, f)$, $V_T(t, f)$ and expressed as [11]

$$\begin{aligned} U_T(t, f) &= X_T(t, f + \frac{\alpha}{2}) \\ V_T(t, f) &= X_T(t, f - \frac{\alpha}{2}) \end{aligned} \quad (8)$$

Using the Equation (8), the time-variant cross spectra correlation between $u(t)$ and $v(t)$ are defined in Equation (9). It turns out to be the time-variant cross spectra correlation between $u(t)$ and $v(t)$, which are $\alpha/2$ frequency shifted versions of process $x(t)$, equal to spectral correlation of $x(t)$ between at $f + \alpha/2$ and at $f - \alpha/2$ at time t . The spectral correlation at time t is called *instantaneous SCF*, $\overline{S_x^\alpha}(t, f)$.

$$S_{uv}(t, f) \triangleq U_T(t, f) V_T^*(t, f) = X(t, f + \frac{\alpha}{2}) X^*(t, f - \frac{\alpha}{2}) = \overline{S_x^\alpha}(t, f) \quad (9)$$

From the instantaneous SCF, an approximation of the SCF is derived by using time-smoothed function [12]

$$S_x^\alpha(f) = \lim_{\Delta t, T \rightarrow \infty} \frac{1}{\Delta t} \int_{-\Delta t/2}^{\Delta t/2} X_T(t, f + \alpha/2) X_T^*(t, f - \alpha/2) dt \quad (10)$$

where T is window size of the time-variant finite-time Fourier transform, and Δt is observation time. In short, the approximation of SCF is integrating the product of two spectral component at each time t within observation time Δt .

The SCF has been derived in two ways so far, resulting in Equation (4) and Equation (10) under continuous time. However, in the real world, discrete analysis is more practical rather than continuous analysis. To derive the discrete version of these functions, we begin with Equation (7). The discrete time-variant, finite-time Fourier transform is given by [7]

$$X_T(t, f) = \frac{1}{\sqrt{T}} \sum_{n=0}^{T-1} x(n + t - \frac{T}{2}) e^{-i2\pi fn/T} \quad (11)$$

The discrete version of time smoothed SCF in Equation (10) is provided as [12]

$$S_x^\alpha(f) = \lim_{T, \Delta t \rightarrow \infty} \frac{1}{\Delta t - T} \sum_{n=T/2}^{\Delta t - T/2} X_T(nT_s, f + \alpha/2) X_T^*(nT_s, f - \alpha/2) \quad (12)$$

where T_s is sampling time. Also, the author in [12] suggested a unique time-smoothing technique for ease of statistical analysis, which avoids the correlation between previous and subsequent instantaneous SCF value:

$$\begin{aligned} \widehat{S}_x^\alpha(t, f) &= \frac{T}{\Delta t} \sum_{n=0}^{\frac{\Delta t}{T}-1} X_T(TnT_s + T/2, f + \alpha/2) X_T^*(TnT_s + T/2, f - \alpha/2) \\ &= \frac{T}{\Delta t} \sum_{n=0}^{\frac{\Delta t}{T}-1} \overline{S}_x^\alpha(TnT_s + T/2, f) \end{aligned} \quad (13)$$

The time smoothing function in Equation (12) is called “Time-windowed” smoothing and the method in Equation (13) is called “time-stepped” smoothing in this research. And to satisfy the statistical reliability, $\Delta t / T \gg 1$ should be met [13] [14].

2.2.3 Properties of the SCF

SCF describes a spectral characteristic that comes from cyclostationarity. A reason why the spectral correlation concept has been studied is that it has some properties which can be used in practical situation resulting in better performance compared to other methods of detecting such as PSD.

One property is that the SCF of same modulation type with different number of possible symbols, such as Binary Phase Shift Keying (BPSK) and Quaternary PSK (QPSK), have different unique features. This is in contrast to the PSD which has identical features on the same modulation type. This property helps to detect expected signal and classify signals according to modulation type. Graphically, four peaks are shown in Figure 1 and two of them are on the $\alpha = 0$ axis and the other two of them are $f = 0$ axis. Among the peaks, two peaks on $\alpha = 0$ and $f = \pm f_0$ are considered as common peak which come up in other schemes where same modulation type (PSK in this example) is used with different number of symbols, such as QPSK, Staggered QPSK (SQPSK). This points out that the two peaks are no longer distinct features of BPSK signal. However, the other two peaks on $\alpha = \pm 2f_0$ and $f = 0$ are distinct compared to other modulation schemes. Figure 1 below shows SCFs of BPSK, QPSK and SQPSK. All plots show similar peaks where $\alpha = 0$, $f = \pm f_0$. However, the other two peaks at

$\alpha = \pm 2f_0$ and $f = 0$ in BPSK signal does not show up in QPSK and SQPSK signal or the height of the peaks are comparatively different from the peaks in SQPSK.

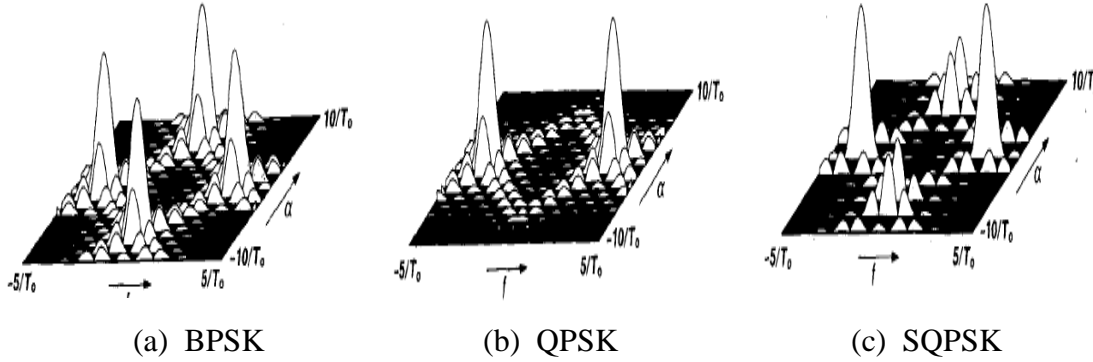


Figure 1. Theoretical SCF magnitude surfaces for BPSK, QPSK, SQPSK with carrier frequency $f_0 = 3.3/T_0$ [15]

Another property is that stationary noise such as AWGN does not exhibit spectral correlation, because the spectral correlation comes from cyclostationarity which is special case of non-stationary process. Therefore, in the limit, the SCF of white noise is identically zero.

In addition, the SCF has phase and frequency information associated with timing parameters, which makes it useful for synchronization. Lastly, the presence of a cyclostationary signal indicates that some parameters such as carrier frequency, symbol rate can be estimated using other spectral components such as cycle frequency [16] [17].

2.2.4 Features of modulated signal

As said in the SCF property section above, each modulation type has distinct SCF features. The feature also varies with the number of possible symbols within same modulation type. We look into SCF feature of Frequency Shift Keying (FSK) modulation

with 2 possible symbols, which is a 2-FSK signal. We will use 2-FSK signals in this research since it has its own SCF feature which comes from only positive frequency band of signal [14] [18].

A phase incoherent FSK signal is represented mathematically as [15]

$$s(t) = \sum_{n=-\infty}^{\infty} q(t - nT_0) \cos(2\pi[f_0 + f(n)]t + \theta_n) \quad (14)$$

where $f(n) = \sum_{m=1}^M \delta_m(n) f_m$ and f_0 is carrier frequency, $q(t)$ is rectangular pulse, T_0 is pulse duration, $\{\theta_n\}$ is an independent sequence and it has uniform fraction-of-time distribution of the interval $[-\pi, \pi]$, $\{f(n)\}$ is stationary and has discrete M-ary fraction-of-time distribution $\{P_m\}_1^M$, and $\delta_m(n)$ is a vector which has one element equal to unity and the others equal to zero for each n [15]. SCF of M-ary FSK signal is given by [15] [19]

$$S_s^\alpha(f) = \begin{cases} \frac{1}{4T_0} \sum_{m=1}^M P_m [Q(f + f_m + f_0 + \alpha/2) Q^*(f + f_m + f_0 - \alpha/2) \\ + Q(f - f_m - f_0 + \alpha/2) Q^*(f - f_m - f_0 - \alpha/2)], & \alpha = \frac{k}{T_0} \end{cases} \quad (15)$$

where $Q(f)$ is Fourier transform of pulse $q(t)$ for all integer k . Interesting thing is that, as can be seen in Equation (15), cycle frequency α where SCF features has non-zero value is not continuous, but discretely distributed with interval of $1/T_0$, the inverse of symbol duration, which is symbol rate [14]. It comes from the fact that the digital carrier modulation has a pulse train with period T_0 which is multiplied by carrier signal as can

be seen in Equation (14). Therefore, cycle frequency α , which is generated by the pulse train, has non-zero magnitudes only at $\alpha = k/T_0$ where k is integer and zero magnitude at $\alpha \neq k/T_0$. In addition, distinct SCF peaks appear at $\alpha = \pm 2kf_d$ where k is integer, f_d is frequency deviation which is a half of frequency separation between peaks [20].

The SCF feature of 4-FSK signal below is visually presented in frequency-cycle frequency plane (bi-frequency plane) in Figure 2.

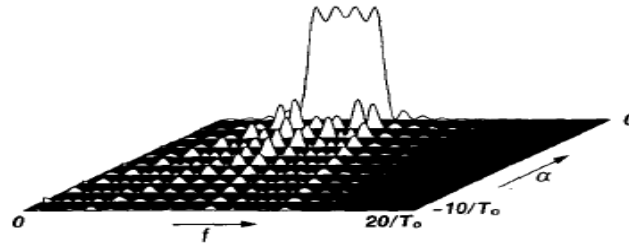


Figure 2. Theoretical Spectral correlation magnitude for 4-FSK signal with

$$\{(f_0 + f_m)T_0\} = \{5, 6, 7, 8\} \quad [15]$$

Figure 2 shows only positive frequency band and negative cycle frequency band of FSK signal with frequency sets $\{(f_0 + f_m)T_0\} = \{5, 6, 7, 8\}$. Separation between peaks at $f_0 + f_m$ is two times the frequency deviation (f_d). That is, the separation between peaks is same with the symbol rate ($1/T_0$) and frequency deviation is same with half of the symbol rate in this example. The SCF features of 4-FSK in Figure 2 are shown to appear at $\alpha = \pm 2kf_d = \pm k/T_0$.

2.2.5 SCF vs. PSD

As noticed in the Wiener relation and Cyclic Wiener relation, PSD is from Fourier transform of autocorrelation and SCF is from Fourier transform of the CAF.

Autocorrelation is special case of CAF when $\alpha = 0$. Thus, it is intuitively assumed that PSD is special case of SCF when $\alpha = 0$. As mentioned above, PSDs, that is, SCF at $\alpha = 0$, of BPSK, QPSK are same, whereas SCFs at $\alpha \neq 0$ have distinct features. In mathematical expression, from Equation (4) and (10), PSDs are derived as below.

$$\alpha = 0; \quad S_x^0(f) = \int_{-\infty}^{\infty} R_x^0(\tau) e^{-i2\pi f\tau} d\tau \quad (16)$$

$$\alpha = 0; \quad S_x^0(f) = \frac{1}{\Delta t} \int_{-\Delta t/2}^{\Delta t/2} X_T(t, f) X_T^*(t, f) dt = \frac{1}{\Delta t} \int_{-\Delta t/2}^{\Delta t/2} |X_T(t, f)|^2 dt \quad (17)$$

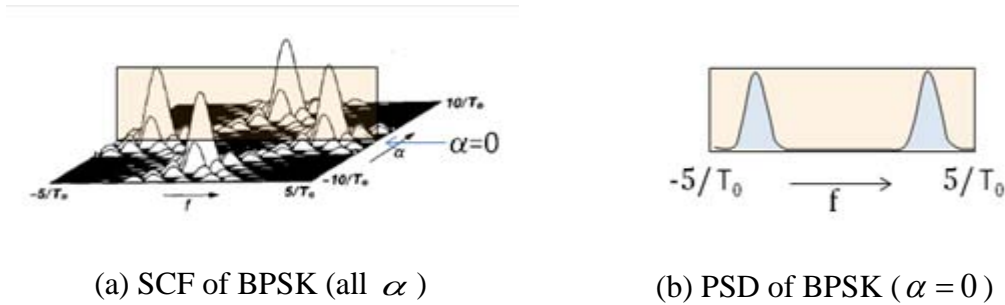


Figure 3 . SCF and PSD of BPSK

Figure 3 shows the relation between SCF and PSD. PSD on the right is a part of SCF when $\alpha = 0$ (red-rectangular in the left), which means that SCF is a generalization of PSD.

2.3 Detection Techniques

As mentioned above, the SCF has practical properties that make the SCF more useful than PSD. Then what exactly makes the SCF better compared to other detection techniques? To answer to this question, three commonly studied and compared techniques are introduced and their advantages and limitations are discussed.

2.3.1 Matched filter detection

Matched filter is a technique for detecting the presence of a signal of a certain shape when assuming that noise is AWGN. Matched filter is the optimal way for signal detection, since it can turn low SNR into high SNR regime so that arbitrary weak signals can be detected [21]. To yield the highest SNR, matched filter controls the impulse response of its filter. To properly control the impulse response, matched filter detection requires *a priori* knowledge of signal, which means that the received signal is a deterministic signal to the receiver. A priori knowledge includes modulation type and order, pulse shaping, packet format, etc. However, since this a priori knowledge is mostly stored in detector's memory, it is not a burdensome process.

Another thing to care about is coherency. Coherency in matched filter designs can be achieved by timing and carrier synchronization, as well as channel equalization [1]. To keep a coherency with existing signal, matched filter detection uses pilots, preambles, synchronization words or spreading codes. TV signals which have a narrowband pilot for audio and video carriers and CDMA systems which have dedicated spreading codes for

pilot and synchronization channels are examples that can be used for overcoming the coherency problem [1].

An advantage of a matched filter in addition to its optimal performance is that it requires $O(1/\text{SNR})$ samples to meet a target probability of error constraint [22]. The number of samples required is related to time performance. Thus, in the case of $\text{SNR} < 1$, matched filter detection can give high processing gain with shorter time than other techniques, such as energy detectors (which requires $O(1/\text{SNR}^2)$ samples [22]). The time performance of matched filter is a lower bound on the sensing time for any possible sensing detector type [21].

The drawbacks of matched filters come from its characteristics. Since it requires *a priori* knowledge of the waveform and coherency with received signal, it is difficult to use in the real world. Practically, this means that in the presence of channel distortion, the receiver must be matched to the convolution of a predetermined impulse response of a filter and the impulse response of a channel which generally can't be identified [23]. Also, a significant disadvantage of matched filters is that they need a dedicated receiver for every different class of signals, which is not applicable to a radio which is expected to detect more than one signal such as cognitive radio because it has to have an ability to detect all the primary user classes.

2.3.2 Energy detection (radiometer)

Energy detection (also known as a radiometer) is non-coherent, which means it is simple to implement because it doesn't require much information for coherent

processing. However it is a suboptimal technique because its performance is not useful in some environments, such as under low SNR.

There are two main ways of performing energy detection. A conventional energy detector consists of a low pass filter to filter out band noise and adjacent signals, Nyquist sampling A/D converter, square-law device and integrator, which is time domain representation of energy detection [21] [24]. A realization of this energy detector is illustrated in Figure 4(a). Another way of performing energy detection is by using a periodogram, which is frequency domain representation [24]. It is also depicted in Figure 4(b). It estimates spectrum via squared magnitude of the FFT. In terms of result, both approaches don't make any difference. However, in terms of utilization, the latter is typically preferred. That is, using pre-filter which should be matched to the bandwidth of the signal makes the time domain approach inflexible compared to the frequency domain approach because frequency domain approach provides the flexibility to process wider bandwidth and detect multiple signals at the same time if the signals have different center frequency, which enables to process arbitrary bandwidth of modulated signals [21] [24].

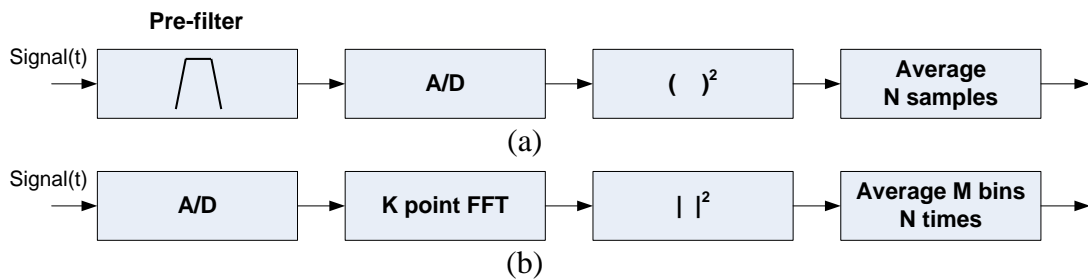


Figure 4. Two approaches of Energy detection. [21]

There are some drawbacks of the energy detector in terms of susceptibility to noise and time performance. The energy detector is susceptible to noise especially in low SNR

environments. Because it is not able to differentiate signal from noise, the signal can be hidden below noise in a low SNR environment, which makes it unable to be detected. This drawback results in the lower SNR “wall”, which is minimum SNR level below which signals cannot be detected, than under other signal detectors. Therefore, the energy detector has good performance only above the SNR wall, and poor performance below it. In addition, under noise uncertainty, there can be a higher probability of false detection [21]. Also, it is susceptible to spread spectrum signals such as direct-sequence spread-spectrum (DSSS) and frequency-hopped spread-spectrum (FHSS) modulation because DSSS has no identifiable spectral feature and FHSS modulated signal itself can be interference [1] [25].

Another disadvantage of the energy detection is that timing or phasing properties of signal of interest cannot be identified from energy detector, which is overcome by using more systems though [25]. In terms of time performance, due to the non-coherent processing, $O(1/\text{SNR}^2)$ samples are needed to meet a probability of detection constraint, which indicates that, in the environment of $\text{SNR} < 1$, the energy detector requires more samples to meet a probability of detection constraint compared to a matched filter which needs $O(1/\text{SNR})$ samples [1]. Thus, under a low SNR environment, a longer time to sense the signal is needed with an energy detector than with a matched filter, but it will be a shorter amount of time than CFDs (discussed next) [26].

2.3.3 Cyclostationary Feature Detection (CFD)

From the properties of SCF discussed before, stationary noise exhibits no spectral correlation, which makes modulated signals that are severely masked by noise be more

effectively detected by CFD using SCF rather than energy detection using PSD [16]. Since matched filter detection is hard to achieve for general signal detection in real world environments, CFD is compared against energy detection. The reason why SCF is used for CFD rather than CAF is similar to talking about the difference between temporal analysis and spectral analysis. Spectral analysis enables CFD to view the received signal within certain range of frequency, not a whole frequency range, which is difficult in temporal view because plenty of signal components of frequencies are superimposed.

One of the advantages of CFD is a high noise tolerance, which means that it has the ability to separate signal from noise. SCF which is used for CFD is described as at coordinates of frequency f and cycle frequency α , whereas the energy detector has only frequency component f . The CFD uses signal features which are discretely distributed in the cycle frequency in the cyclic spectrum, already mentioned in Section 2.2.4, even if continuous distribution is exhibited in the power spectrum. This indicates that overlapping features in the power spectrum of signals can have non-overlapping features in the cyclic spectrum, that is, SCF features are not overlapped due to its discretely distributed property [25]. This characteristic is applied to background noise which is assumed to have no cyclic feature at $\alpha \neq 0$ and, therefore, is used to analyze signals at a nonzero cycle frequency where only a signal of interest feature which has cyclostationarity is expected to appear and the noise to disappear. Such analysis will expose the cyclostationary features of a signal without any other features caused by background noise except measurement noise [25]. Another advantage of CFD is that it is

able to identify modulation types by examining SCF features at $\alpha \neq 0$ since these features often change with modulation type.

In [1], the author insists that SCF has its unique features even under low SNR environments using AWGN as a noise. In high SNR environments ($\text{SNR} > 1$), when a signal strength is larger than noise strength, PSD and SCF show their unique features in bi-frequency plane as in Figure 3 (a). However, in low SNR environments ($\text{SNR} < 1$) when noise strength is larger than signal strength, PSD is hidden by noise and its unique feature is not visible. Thus, it is impossible for energy detector (which uses PSD) to know whether the signal exists or not. Whereas, SCF features when $\alpha \neq 0$ is still visible regardless of noise strength. From the fact that PSD is a part of SCF when $\alpha = 0$, the author says that, only when $\alpha = 0$, large noise appears and hides a PSD feature of a signal and, in areas where $\alpha \neq 0$, large noise does not appear and SCF features of the signal are still visible without being buried under noise. Thus the CFD detects the target signal by inspecting not the SCF features in $\alpha = 0$ region but SCF features in $\alpha \neq 0$ region, because SCF features in $\alpha \neq 0$ area are not buried by noise which has little spectral correlation. Furthermore, by inspecting the locations and relative magnitudes of the peaks at $\alpha \neq 0$, the modulation type can also be identified.

However, the CFD has a disadvantage in the computation aspect. It can be easily seen that the CFD using the SCF is more complex to calculate than energy detection because the PSD (which can be used in energy detection) is only one part of the SCF. In other words, the PSD can be represented using a 2-dimensional plot whereas the SCF requires a 3-dimensional plot (like Figure 3). The PSD only considers one parameter (frequency)

but SCF considers two parameters (frequency and cycle frequency) which give intuition that the SCF takes up more calculation than PSD.

The computational complexity of SCF depends on the resolution of frequency f as PSD does. However, increment of the FFT resolution has larger effect on the computational complexity of SCF than that of PSD. Figure 5 below shows the computational process of the SCF. The detailed operation of N-point FFT and correlation is shown in the rectangle. In terms of complex multiplier, the number of multiplier in SCF scales as $O(N^2+N\log N)$ whereas that of energy detection scales as $O(N)$, where N is the resolution of FFT [26] [20]. Note that this $O(N)$ is computational performance, that is, the number of operations needed at certain samples, whereas $O(1/\text{SNR}^2)$ is time performance which is that how many samples are needed to meet certain detection performance under certain SNR level.

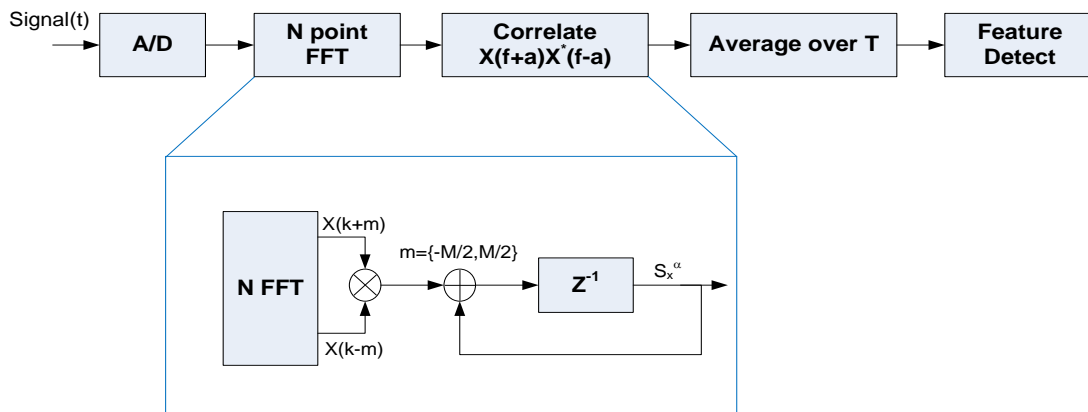


Figure 5. Implementation of a cyclostationary feature detection [20]

Even though a computation complexity problem exists for CFD, there are papers that try to mitigate the number of operations, making implementation of the CFD method to hardware for real time estimator practical. One technique is to only estimate the SCF on

the supported area where SCF has distinctive non-zero magnitude response [27] [28] [29]. This reduces the number of operations and makes real-time processing feasible. However, this paper assumes that the signal is digitally modulated and the detector already knows which part of SCF will have these distinctive features. Locations of modulated signals that exhibit distinctive features are studied in detail in [15]. Location of features of BPSK signal is covered in Section 2.2.4.

2.4 Channel Noise Analysis

We have discussed the SCF's definition, properties and its application to signal detection. However, in the real world, a signal is distorted by the noise, which means that noise can affect the cyclostationary feature of a real world signal.

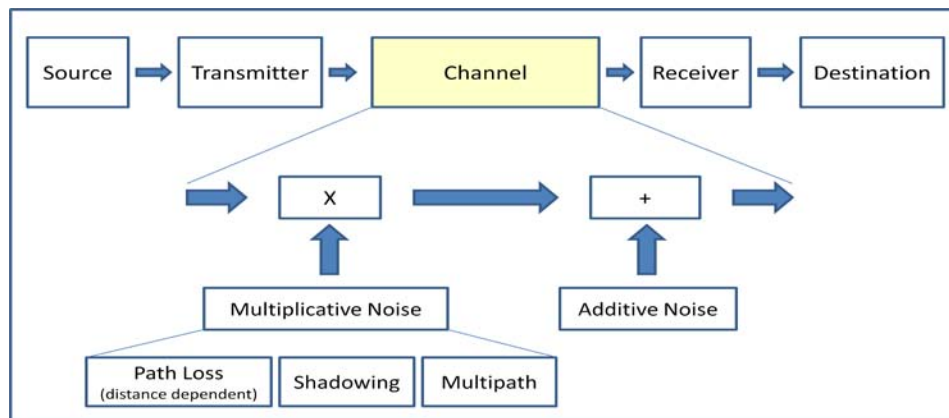


Figure 6. Noise in the wireless channel [30]

Real world wireless channels are not so simple that they only have AWGN. Noise that modifies the signal in either predictable or unpredictable way in the wireless channel can be divided into two types of noise: additive noise or multiplicative noise [30]. Figure 6 describes noise in the wireless channel.

Additive noise is generated within the receiver itself, such as thermal noise, or from external sources like atmospheric effects, cosmic radiation and interference from other transmitters and electrical devices. Environmental noise and thermal noise from the receiver itself are mostly white noise with low strength and unavoidable, which spreads over whole frequency bands with almost same noise strength, preserving correlation structure. Other additive noise from artificial sources such as co-channel interference tends not to be white which can cause SCF change.

Multiplicative noise is generated from diverse processes encountered by transmitted signal waves on their way to receiver, which means that it is involved in propagation processes of transmitted signal from transmitter to receiver. Reflection, absorption, scattering, diffraction and refraction are representative processes which occur during propagation and can be said to be causes of multiplicative noise. The multiplicative noise is further divided into three types of fading; path loss, shadowing (slow fading), and multipath fading (fast fading). Multiplicative noise appears to be time-varying and location varying processes making it hard to predict its effect [30].

Figure 7 describes real world received signal and its multiplicative noise components. Figure 7. Multiplicative noise components in real world : Path loss, Shadowing, MultipathFigure 7 (a) describes received signal. The signal is a resultant signal of going through all the multiplicative noise. Each of the other plots shows each multiplicative component effect.

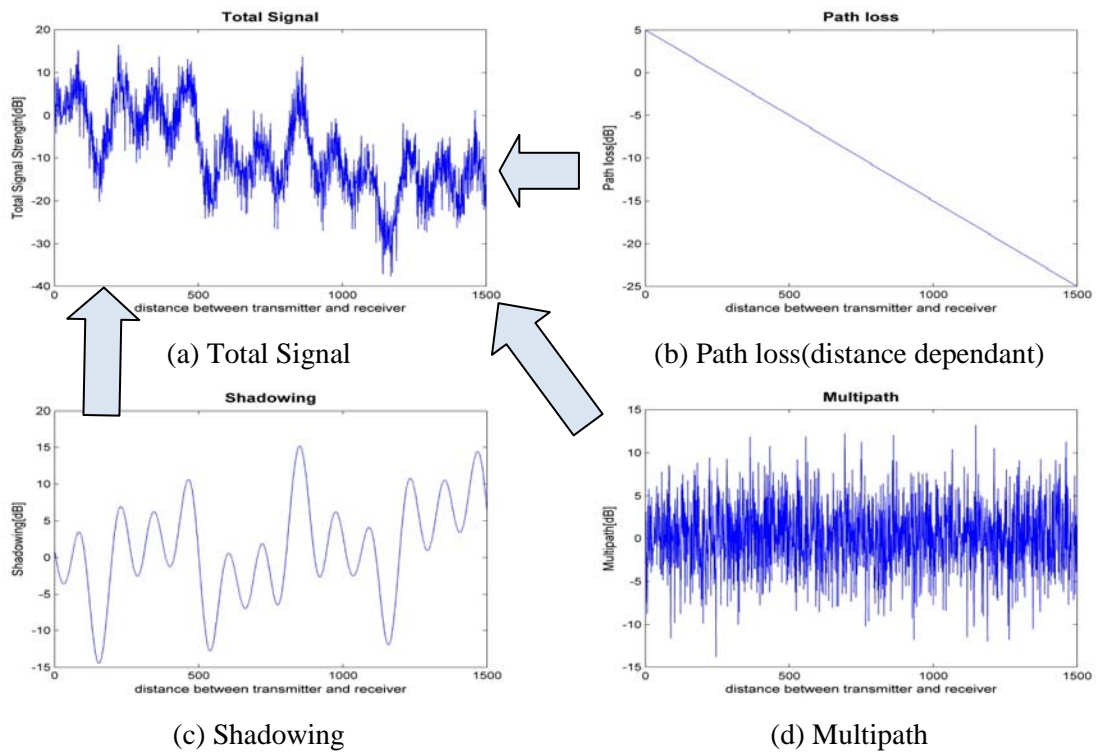


Figure 7. Multiplicative noise components in real world : Path loss, Shadowing, Multipath

- *Path loss* (distance dependant) : Mostly refers to signal power loss from distance increase between transmitter and receiver. The path loss increases logarithmically as distance increases. The plot on the top right in Figure 7(a) describes path loss under the dB scale.
- *Shadowing* (slow fading) : It is also referred to as a long term variation, large-scale fading and generally caused by obstructions of the Line Of Sight (LOS) signal by buildings, mountains, etc [31]. Shadowing changes faster than path loss and has variation generally up to 20 dB [30]. The shadowing is illustrated in Figure 7 (c) on the bottom left. It is seen that the variation of amplitudes are slower than the right one, which is from

multipath fading discussed next. That's why it is also known as "slow fading".

Diffraction is main loss components of shadowing.

- *Multipath* (fast fading) : Also known as short term variations, or small scale fading. Multipath is caused when more than one version of the transmitted signal arrive at the receiver at slightly different times [32]. Each version of the transmitted signals act like interference and they can result in having destructive or constructive effect on the signal. This phenomenon is due to propagation processes such as reflection, diffraction, refraction and scattering [31]. And it often results in rapid variation of the amplitude of the transmitted signal over a short time or travel distance, which is the reason why it is called "small scale fading" [30]. The fast variation can be seen in Figure 7 (d) on the bottom right. Two representative multipath models are Rayleigh fading and Rician fading. Rayleigh fading is to describe propagation in heavily built-up urban environments without LOS whereas Rician fading is utilized in environments where multipath occurs with a LOS path, that is, one version of signal is much stronger than others [33].

The basic stochastic path loss estimation model below, called "log-normal shadowing", is provided to model the additive, multiplicative noise components built through empirical measurements [32]. That is, this model here considers not only distance dependent path loss but also effects of shadowing and multipath.

$$PL = \overline{PL}(d_0) + 10n \log_{10}\left(\frac{d}{d_0}\right) + X_\sigma \quad (18)$$

where \overline{PL} is the average path loss in decibels, n is the path loss exponent which is the rate at which the path loss increases with distance increases, d_0 is the close-in reference distance and d is the transmitter-receiver separation distance. X_σ is a zero-mean Gaussian distributed random variable (in dB) with standard deviation σ which also varies depending on environments [32]. This statistical distribution random variable is used to show unpredictable shadowing and multipath effects. $\overline{PL}(d_0)$ is considered as a constant path loss factor at reference distance d_0 . Parameter d stands for distance and the value of n is assigned different values depending on environment.

Table 1 shows path loss exponent values for different environments. From Table 1 and Equation (18), the fact that location (environment) and distance affect the path loss is easily noticed. Overall, the path loss exponent n and X_σ indicate the level of multipath and shadowing. Distance is mainly involved in path loss.

Table 1. Path Loss Exponents for different environment [32]

Environment	Path loss exponent, n
In building line-of-sight	1.6 to 1.8
Free space	2
Obstructed in factories	2 to 3
Urban area	2.7 to 3.5
Shadowed urban area	3 to 5
Obstructed in building	4 to 6

The log-normal shadowing model is built based on empirical experiments using the PSD of the signal, showing the effects of noise on signal power. However, the PSD is used for energy detector which has been shown to have worse performance under those

multiplicative noise effects [34]. There has been no research on a SCF-based path model to identify the effects of noise like the PSD based log-normal shadowing model above. Therefore, the characteristics of SCF under path loss, shadowing, multipath need to be investigated by varying distance and locations.

2.5 Discussions

There has been a lot of research focused on analyzing the real world effect of noise on signal strength, especially multiplicative noise, by performing empirical experiments based on PSD. In [35], the author tried to analyze the RSS measurements statistically under shadowing and multipath in an indoor environment. He figured out the proper number of replication for measurement, determining that 40-replication seemed to be enough trials to convergence on a mean and standard deviation. He also compared theoretical second order statistics with the empirical ones, which are level crossing rate (LCR) and average fading duration (AFD), to show variations of RSS measurements in real world. Even though this paper is on signal strength which is based on PSD, methodologies used here can be applied to studying SCF based path loss effect such as determining the number of trials for statistical analysis.

From an analytical perspective, in [12], the authors derived probability distribution of SCF and PSD analytically, showing that, under AWGN, the SCF of a signal which follows Gaussian distribution has better detection performance than PSD. In addition, they show that observation time affects the SCF feature values. As observation time increases, the SCF variance and mean of AWGN decrease. The decrease of the mean of AWGN makes the SCF feature distinct in low SNR environments. In the same context,

[7] showed that SCF floor gets lower as the observation time gets longer by simulation, which indicates that SCF feature can be detected under lower SNR environment with longer observation time, shown in Figure 8.

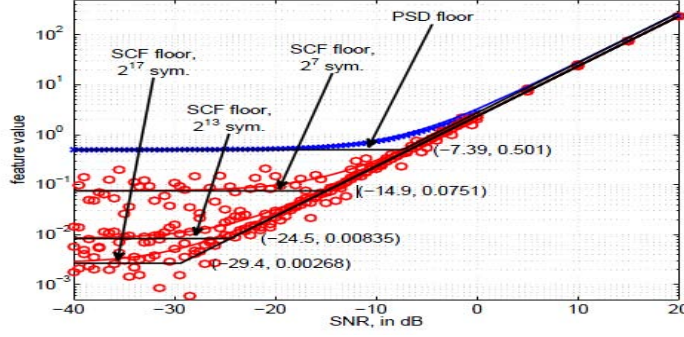


Figure 8. SCF of BPSK under different SNR/observation time compared with PSD [7]

Table 2. Statistical Properties of Time Smoothed and Instantaneous PSD/SCF [12]

		Dist.	Mean	Variance
1	$S_c(t, k)$	χ_2^2	σ_c^2	σ_c^4
2	$S_{x+c}(t, k)$	χ_2^2	$\sigma_x^2 + \sigma_c^2$	$(\sigma_x^2 + \sigma_c^2)^2$
3	$\overline{S_c}(k)$	\mathcal{N}	σ_c^2	$\frac{N}{T} \sigma_c^4$
4	$\overline{S_{x+c}}(k)$	\mathcal{N}	$\sigma_x^2 + \sigma_c^2$	$\frac{N}{T} (\sigma_x^2 + \sigma_c^2)^2$
5	$re\{S_c^\alpha(t, k)\}$		0	$\frac{1}{2} \sigma_c^4$
6	$ S_c^\alpha(t, k) ^2$		σ_c^4	$4\sigma_c^8$
7	$\overline{S_c^\alpha}(k)$	\mathcal{CN}	0	$\frac{N}{T} \sigma_c^4$
8	$re\{\overline{S_c^\alpha}(k)\}$	\mathcal{N}	0	$\frac{N}{2T} \sigma_c^4$
9	$re\{\overline{S_{x+c}^\alpha}(k)\}$	\mathcal{N}	σ_x^2	$\frac{N}{T} (\sigma_x^4 + \sigma_x^2 \sigma_c^2 + \sigma_c^4)$
10	$ \overline{S_c^\alpha}(k) ^2$	χ_2^2	$\frac{N}{T} \sigma_c^4$	$\left(\frac{N}{T}\right)^2 \sigma_c^8$

Table 2 above shows statistical properties of instantaneous / time smoothed PSD and SCF in [12]. The author used the time smoothing method described in Equation (13) in Section 2.2.2 to calculate the SCF.

S^α is SCF and S is PSD. Instantaneous SCF and PSD has parameter t . x denotes signal of interest with Fourier transform variance σ_x^2 and c denotes AWGN with variance σ_c^2 .

There has been research on SCF under AWGN and multipath fading. In [36], the author used a “cyclostationary signature” which is a unique identifier or watermark intentionally embedded to signal and identified through SCF. He proved using simulation that the cyclostationary signature is sensitive to time variant Rayleigh multipath. A method using multi-feature signatures was provided to overcome this sensitivity. On the other hand, [37] showed AWGN and multipath impacts on SCF through simulation. The signal detection performance of SCF under Rayleigh fading and AWGN is almost same with the performance under only AWGN except when SNR is below -15dB, which means the Rayleigh fading doesn't have critical effect on SCF performance when the SNR is above the -15 dB. In [13], the authors proposed a method to improve CFD using the fact that SCF is robust to slow multipath fading, low SNR environments and is insensitive to unknown prior knowledge of received signal by simulation.

Some papers have used real experiments to understand the SCF in a limited manner. In [38], the author presented the real world performance of CFD in the form of SCF through hardware implementation overcoming its hardware limitation such as sampling clock offset by partially coherent feature processing. The author tried to figure out the

performance of his CFD with experimental approach. But noise used in his research was synthetic stationary white noise, which does not fit our research goal. In addition, the author figured out that the CFD outperformed an energy detector under out of band interference using a real world signal.

In addition, through empirical experiments, the author in [31] showed that under multipath fading with static and dynamic states the SCF still shows its cyclostationary features in the $\alpha \neq 0$ regions. However, under multipath fading with dynamic condition, SCF has a larger number of periodic components that are not multiples of a fundamental frequency, which indicates that the resultant signal can be considered as polycyclostationary [31]. In our research, dynamic states are not considered. These studies using real world experiments are not enough to characterize SCF features of modulated signals in real world. [38] more focuses on implementing SCF on hardware and figuring out its limitation and [31] more focuses on stationary analysis under multipath and shadowing effects.

Even though there has been research on SCF under noise, they are limited in the aspects of its environments (AWGN, multipath fading), its evaluation technique (theory, simulation, real measurement) and its scope. Therefore, the characteristics of SCF with real world signal under channel noise need to be investigated in detail.

III. Methodology

3.1 Introduction

This chapter discusses the methodology of the research. To do this, the problem is introduced and the goal of the research is defined with expected result of the research. Next, a detailed methodology is discussed defining the system boundaries and their components, parameters and factors. Finally, the test bed is described and the experimental design and evaluation techniques are covered.

3.2 Problem Definition

3.2.1 Problem

In Chapter 2, cyclostationarity and the SCF were introduced along with the properties, performance of SCF over PSD and different SCF features of some modulation types. The SCF features of a FSK signal were presented from a theoretical perspective. Furthermore, channel noise was introduced with recent research on the effects of additive / multiplicative noise and interference on the SCF features from a theoretical, simulated and experimental perspective.

Even though there has been research on effects of channel noise on the SCF, most of this has been done from the perspective of AWGN and multipath fading. In order to understand comprehensively the effect of additive and multiplicative noise on SCF under real world uncertainty, the properties of the SCF under real world channels needs to be investigated in detail. The investigation into the real-world effects of noise on the SCF features would help to validate the utility of cyclostationary feature based signal

detection. There has been no research on finding SCF feature characteristics in terms of the path loss model, varying distance and location, as done in PSD. Thus, it is meaningful to characterize the SCF feature using the “path loss” approach. In addition, the performance of SCF under low SNR environment, while analyzed theoretically, should be examined experimentally. Lastly, observation time has been shown to improve the SCF feature statistic components affecting the SCF feature levels of noise floor [7] [12], but a real world investigation into the observation time need to be performed to validate the argument.

3.2.2 Goals and Hypothesis

The goals of this research are

- To identify and characterize the difference between the theoretical and actual cyclostationary features of modulated signals under channel noise in terms of path loss, shadowing and multipath under various locations and transmitter / receiver separations.
- To determine the performance difference between SCF over PSD under low SNR environment with real world signal.
- To observe the effect of observation time on the SCF statistics.

It is expected that path loss model of the SCF will be similar to the PSD path loss model with lower noise floor because SCF comes from multiplying two frequency components which belong to PSD as well. The real world performance of SCF detection is not expected to be as good as theory since current noise model such as AWGN may be different from real world noise and there can be some unexpected correlations between

noise and signal, and among noise. Lastly, longer observation time is expected to decrease the variance of SCF feature and lower the noise floor level.

3.2.3 Approach

Equation (13) is used to obtain SCF feature values in experiments by giving particular α , f values. To identify the SCF feature of modulated signal in a real world environment (including channel noise) and compare the feature response against theory, various configurations of real world environments will need to be designed to capture various noise conditions. Since these environmental conditions are not able to be controlled directly, they will be controlled indirectly by varying the transmitter / receiver location, separation distance and transmit power. This will affect the SNR as well as the channel noise, interference, multipath conditions and path loss.

Specifically, the path loss of SCF features is measured by varying the transmitter / receiver separation distance in different locations. This helps to understand the effect of channel noise at fixed transmit power and fixed observation time. The resultant SCF path loss is compared to PSD path loss. To observe the SCF feature under low SNR, the SNR is changed by controlling the transmit signal strength. Performance of SCF under low SNR is compared with performance of the PSD. The observation time is varied by controlling time smoothing degree of SCF in signal processing part. SNR and observation time are varied at fixed distance and fixed location. Results of the experiments on the effect of SNR and observation time on SCF are compared with analytic, simulation-based results done previously in [7].

3.3 System Boundaries

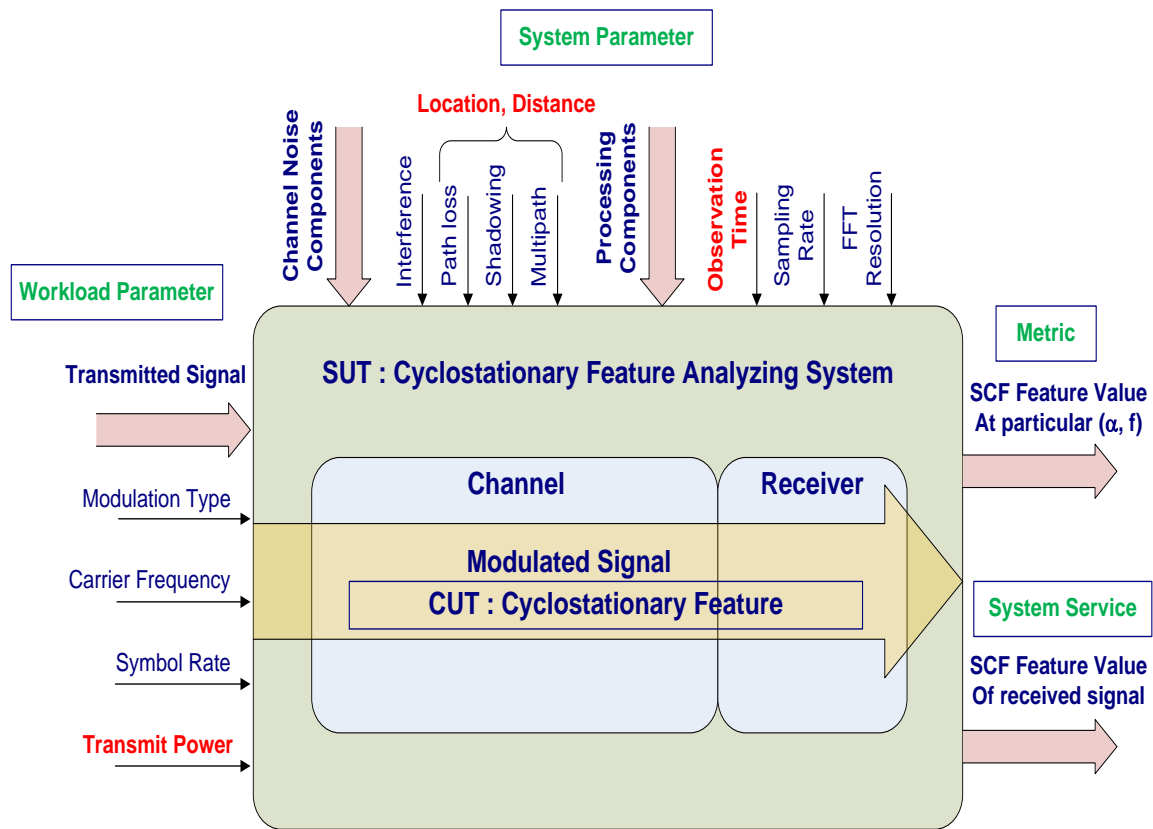


Figure 9. System Under Test (SUT)

The System Under Test (SUT) is a “Cyclostationary Feature Analyzing System” and it consists of a receiver and a channel which is a medium of the signal. The receiver of the system receives a signal transmitted through the channel and analyzes it using the SCF. The receiver includes a Software Defined Radio (SDR) which receives signal and a laptop which runs SCF codes to analyze the received signal using Simulink in MATLAB. The channel can be affected by additive / multiplicative noise such as interference, path loss, shadowing, multipath (other dynamic effects such as Doppler and hardware noise

are not considered). The Component Under Test (CUT) are the cyclostationary features of modulated signals in the channel.

3.4 System Services

The service the system provides is to analyze the cyclostationary features of the received signal using the SCF. Outcomes of system are SCF values of received signal at certain frequency f and cycle frequency α coordinates in $\alpha \neq 0$ area. The outcome value would be used to determine the presence of expected signal in the channel if the system is used in signal detector. However, only the SCF value is the outcome in this system.

3.5 Workload

A workload is a request for system services, which means that the workload in this system is a particular configuration of transmitted signals in a channel. In the research, the signal configuration is the set of components that define the signal, which includes modulation type, carrier frequency, symbol rate, power strength. These components affect the SCF feature values of the received signal. All other things that affect the feature value but are not part of the workloads (such as observation time) belong to system parameters. Specifically, the workload consists of:

- *Modulation type*: The modulation type that we use for the research is 2-FSK, which has SCF features not only from spectral components at both positive and negative frequency band but also from spectral components only at either positive or negative frequency band FSK modulation requires an additional frequency

configuration component which is frequency deviation (f_d). The f_d in our experiments is set to 20 KHz, which is same with symbol rate.

- *Carrier Frequency:* 2.45GHz \pm 50MHz Industrial, Scientific and Medical (ISM) band is used. The reason why the band is chosen is that common communication such as cellular phone, Wi-Fi and FM radio communication in military uses frequency bands higher than 500MHz and lower than 2.5GHz. Within this range there are two ISM bands (2.45GHz and 915MHz) and the 2.45GHz band is chosen and the carrier frequency is 2.45 GHz.
- *Symbol rate:* Symbol rate should be determined considering the available bandwidth, because symbol rate is proportional to bandwidth. In practice, bandwidth is roughly 1.8 times as wide as symbol rate [39]. Available bandwidth is ± 50 MHz in the 2.45GHz ISM band. In addition, available bandwidth of receiver is 25 MHz due to its decimation function. Then maximum symbol rate is 13.89 MS/s (≈ 25 MHz / 1.8). Because taking the whole available bandwidth is not practical and causes much more possibility to be interfered and processing high bit rate can burden the processor, the symbol rate, 20 KS/s, is chosen to have much narrower bandwidth about 36 KHz.
- *Transmit power:* Even though it is a component of the signal configurations, because transmit power is varied only to differentiate SNR, it is discussed in Section 3.8, which is discussed later.

3.6 Performance Metrics

In all experiments, the time-smoothed SCF value at a particular position in the frequency-cycle frequency plane is measured. Equation (13) is used to obtain the (f, α) position in the SCF. A magnitude peak should show up at particular position if the signal is present without any extenuating environmental conditions. The theoretical (f, α) coordinates of the SCF feature for 2-FSK are used (discussed in Section 2.2.4), where $f = f_c - f_d$ and $\alpha = 2f_d$, where f_c is carrier frequency and f_d is frequency deviation.

3.7 System Parameters

System parameters are parameters within the system boundary that affect the SCF feature values of the received signals. All parameters except configuration components of the transmitted modulated signal (which are workloads) belong to the system parameters. System parameters include channel noise components (such as path loss, shadowing, multipath, interference) and processing components at receiver (such as observation time, FFT resolution, sampling rate etc.).

Detailed control of the channel noise is difficult to accomplish whereas control of the processing parameters can be directly manipulated. Controlling the channel noise components are difficult in real world. Because locations and distance reflect the degree of the noise effects such as path loss, multipath, shadowing, these are varied as can be seen in path loss model in Section 2.4. In other words the levels of path loss, shadowing, and multipath are assigned indirectly by the choice of transmitter and receiver location and separation. Interference is not controlled in the research, but significant interference

on the frequency band where the modulated signal is transmitted is prohibited by inspecting the band using PSD before the experiment. Significant interference in this research indicates the interference from external source which has stronger power than background noise. The location and distance are discussed later in Section 3.8, because they are varied during experiments.

For processing components, FFT resolution and sampling rate are fixed, and observation time is varied. The fixed system parameters are given here.

- *FFT Resolution:* The FFT resolution in Simulink tool (which is used in the experiment as a signal processor) is 512 samples. The USRP2 (discussed more in Section 3.10), which is the signal receiver, transmits a data frame of size 358 samples to the Simulink signal processing block set. Simulink can only run FFTs with a resolution of power of 2. If the resolution is smaller than the number of samples of a frame, which is 358, the samples lose information of signal. However, if the resolution is greater than or equal to 358, it does not affect the information of the received signal. In the case of the resolution being greater than the number of samples, FFT performs zero-padding which does not decrease the information [40]. Therefore, resolutions greater than or equal to 512 are possible and the smallest one of them is chosen, which is 512, to avoid memory issues. Considering sampling rate and symbol rate which will be used in this research, 12.8 symbols are expected to be covered by 512 samples.
- *Sampling rate:* Sampling rate should be determined according to bandwidth available, obeying Nyquist theory not to cause aliasing issues. The bandwidth of

received signal depends on symbol rate of transmitted signal. Because the symbol rate is 20 KS/s, the bandwidth is about 36 KHz ($= 1.8 \times 20K$). Considering frequency deviation, which is 20KHz, sampling rate should be greater than 112 KHz ($= (36K + 20 K) \times 2$) from Nyquist theory. And USRP2 basically samples signal at 100MS/s and decimates the samples by the decimation factor which ranges from 4 up to 512. In the research, decimation factor of 125 is selected resulting in sampling rate 800 KS/s ($= 100M/s$ divided by 125), which easily satisfies the Nyquist requirement.

3.8 Factors

Factors are a subset of the system parameters and workloads that are varied during the experiments. In order to identify the difference between real world and theoretical SCF features, that is, in order to identify effects of real world transmit channel, we vary the levels of the transmitter / receiver separation distance as well as their locations. This is because separation distance and location affects the path loss, shadowing, and multipath resulting in differentiating channel noise as can be seen in log-normal shadowing path loss model discussed in Section 2.4.2.

The SNR is varied at the fixed distance and location to examine its better performance than PSD under low SNR environments from theoretical and simulation-based researches.

Lastly, the observation time is changed to verify how it affects the statistic components of SCF feature values, the mean and variance, compared with theoretical result [12] and to verify that the noise floor of SCF is lowered as the observation time

increases improving performance of SCF under low SNR environments [7]. Observation time means that how many samples are used to get one SCF value in signal analysis, thus the observation time is controlled by the number of samples, also can be said as time smoothing degree. The levels of each factor are varied as below.

- *Distance*: A range of separation distance between transmitter and receiver is from 30 cm to 1500 cm. Most research on path loss is categorized based on coverage. Common categories (or system types) include: satellite fixed links, terrestrial fixed links, mega-cells, macro-cells, micro-cells, and pico-cells [30]. Because the system types except pico-cells have much wider coverage than the coverage in our research, the pico-cell system can be most appropriate system for our research. However, because most pico-cell systems are characterized for indoor environments, our research (which uses outdoor as well as indoor locations) is not truly a pico-cell system. Even though our research is not fit for any types defined in [30], because signal detection using SCF under indoor and outdoor with close separation distance can be applied to various applications such as wireless sensor networks, the distances used in the research can be said to be meaningful.
 - 15 measurements points are chosen between 30 cm to 1500 cm.
 - Specific points for measurements are determined by evenly spacing the interval between measurement points in log-space.
 - Distance from the receiver to each measurement points are :
30, 40, 52, 69, 92, 121, 160, 212, 281, 371, 491, 649, 858, 134, 1500 (cm)

A separation distance is fixed when experiments on SNR and observation time are being executed as 150 cm.

- *Location*: 8 locations are chosen. As each type of environment has different path loss exponent n , the location factor here is varied corresponding to the environments in the Table 1 as Table 3 below.

Table 3. Location Factor

Environment		Locations	
In-door	In building line-of-sight	LOS	Hallway, Auditorium (2 locations)
	Obstructed in factories	non-LOS	ANiMaL lab (1 location)
	Obstructed in building	non-LOS	Hall way (1 location)
Out-door	Free space	LOS	Anechoic chamber, Parking lot (2 locations)
	Urban area	LOS	Between buildings in AFIT (1 location)
	Shadowed urban area	non-LOS	Next to building (1 location)

When experiments on SNR and observation time are being executed, the location used is Class room.

- *Transmit power*: SNR at a fixed distance, constant fading and interference can be varied by the transmit power, which means that SNR is controlled by varying received signal power with fixed noise strength. Received signal power should be measured to get exact SNR. Transmit power is measured using power equation in [7], which is

$$P_{PSD} = \int_{f_c - f_b}^{f_c + f_b} |Y(f)|^2 df \quad (19)$$

where $y(t)$ is signal at center frequency f_c with bandwidth $2f_b$. After transmit power and noise power are measured and calculated, SNR in dB scale is derived using

$$SNR(dB) = 10 \log_{10} \left(\frac{Power_{transmit}(mWatt)}{Power_{noise}(mWatt)} \right) = Power_{transmit}(dBm) - Power_{noise}(dBm) \quad (20)$$

Meanwhile, measuring a signal power can be a problem where the signal power is less than or equal to noise power because the signal is hidden by noise. Thus, received signal power is measured indirectly in low SNR environment using the fact that the transmit power can be controlled through signal generator as shown in Figure 10.

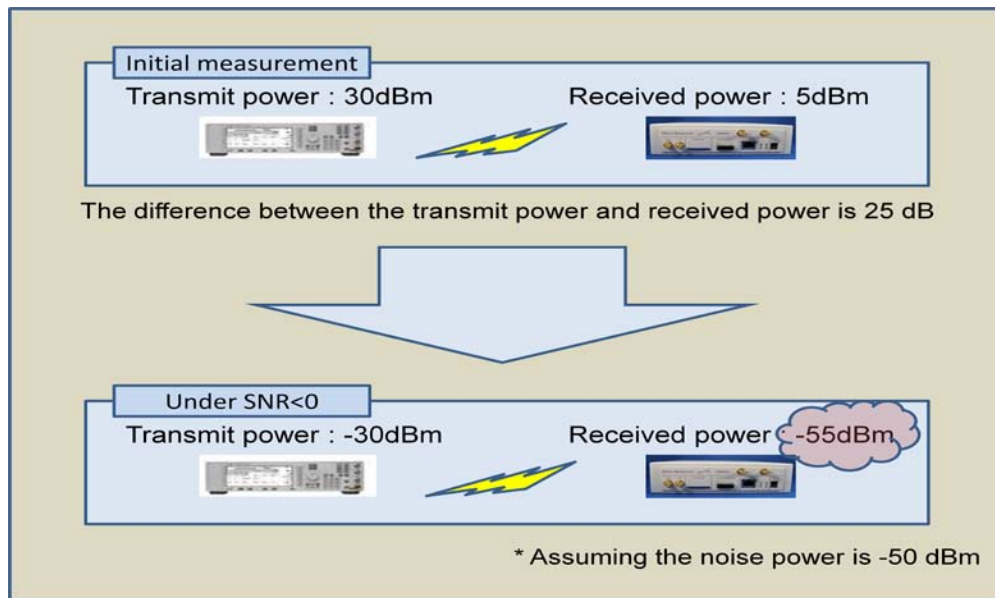


Figure 10. Estimating the received signal power under SNR < 0 (dB)

Initially, in high SNR environment, transmit power and received signal power are measured at particular distance and the difference between transmit power and received signal power is identified, for example, as k (dBm). Then, at the same distance and location, the received signal strength is easily estimated to be (transmit power $- k$). In this way, the signal power levels under noise power level are estimated.

By doing this, SNR is varied from -40 dB to 25 dB and measurements are executed in every 2.5 dB increase in low SNR environment and in every 5 dB increase in high SNR environment (22 levels).

However, the transmit power is varied only for identifying performance of SCF in low SNR environment. Thus, during other experiments, the signal power is fixed with -45 dBm strength in order to have both high and low SNR environments (SNR > 0 and SNR < 0 [dB]) within 15 m separation distance between transmitter and receiver.

- *Observation time*: Observation time is indicated by the number of samples. The range of observation time is from 512 (= 512×1) samples to 2097152(= 512×4096) samples. Experiments for identifying the effect of observation time are done with fixed location, fixed distance.
 - Observation time settings (7) : 512×1 , 512×4 , 512×16 , 512×64 , 512×256 , 512×1024 , 512×4096 (samples)

Observation time is also varied for path loss experiments and SNR experiments. For path loss experiments, observation time is varied to see whether there is an effect on path loss exponents or not. For SNR experiments, observation time is varied to see whether there is an effect on SNR level of noise floor, which is to be compared with Figure 8 in Section 2.5.

3.9 Evaluation Technique

Direct measurement is used as an evaluation technique in the research according to the goal of the research, which is to investigate the real world performance of SCF feature.

Measurement technique can have low accuracy with unexpected uncontrolled environmental condition where there is such a strong interfering power signal that the signal affects the result. By inspecting a frequency band of interest through PSD, the chance that the results are not affected by particular signal interference is minimized.

3.10 Test bed

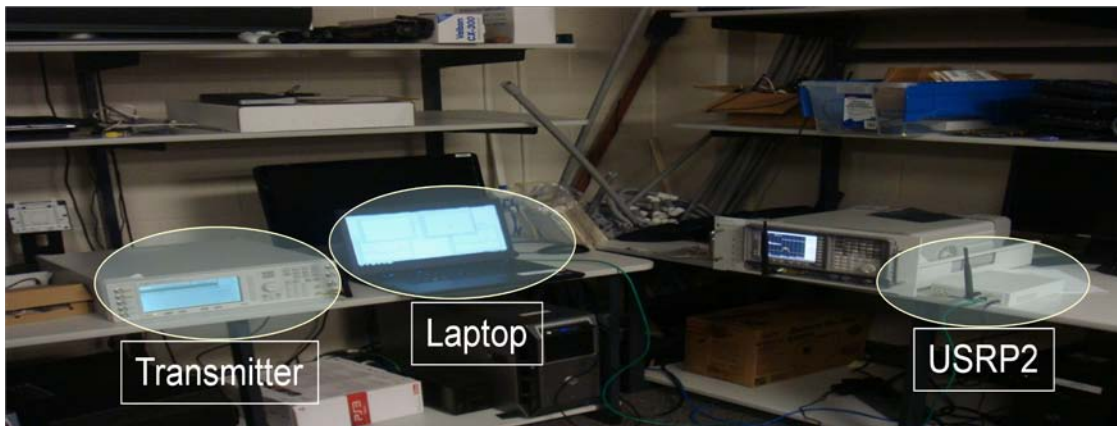


Figure 11. Test bed for experiments

The test bed consists of:

- *Transmitter*

An Agilent E4438C, ESG Vector Signal Generator is used. It generates 2-FSK signal with controllable symbol rate and transmit power. During the research, it generates 2-FSK signal with 20 KS/s symbol rate at 2.45 GHz carrier frequency varying the transmit power.

- *Receiver*

A Universal Software Radio Peripheral 2 (USRP2) is used as a receiver. The USRP2 is a Software Defined Radio (SDR) with capability to perform a limited number of high speed, high precision general purpose signal processing tasks such as decimation, interpolation, digital up conversion and down conversion. A Field Programmable Gate Array (FPGA) is utilized for providing high speed processing tasks in the USRP2. Other signal processing tasks such as modulation, demodulation, and filtering are performed on a host computer [41] [42].

A daughterboard, the RFX 2400, which covers from 2.3 to 2.9 GHz frequency range, is used. In the experiments, USRP2 continuously receives a 2.45GHz signal at 100MS/s sampling rate and decimate the sampled signal with the decimation factor 125, resulting in 800 KS/s sampling rate. It also performs downconversion on the signal to the baseband in the end, making the signal centered at 0 Hz, which needs some adjustment on the sampled signal because down conversion makes the SCF features of modulated signal invisible. After sampling, decimating and downconverting the received signal, it sends the data to

a laptop via Gigabit Ethernet Cable in a frame, size of 358 samples. The transmitter and receiver are located at the height of 110 cm above the floor.

- *Laptop running Simulink*

A host computer connected to USRP2 is a laptop running Simulink in MATLAB, which receives transferred signal data in frame format, processes the data, shows / records the SCF values in real time.

The laptop is a Dell Precision M4500 running Windows 7 Professional with Intel Core i7 processor, 8G RAM, 320G hard drive. Simulink in MATLAB R2010b running in the laptop provides USRP2-Simulink block set which interfaces with USRP2 devices, allowing simulation and development work for SDR related work in real time. Simulink provides not only interface with USRP2, but also other signal processing blocks and embedded block which users can customize the function of block using MATLAB code.

During the research, USRP2 Simulink block set receives data continuously from USRP2 and send the data to signal blocks and embedded blocks which analyzes the received data by calculating and recording the SCF values at the particular (f, α) position in real-time.

- *Simulink Block Setup*

The Simulink blocks in Figure 12 below describe how the data flows are analyzed. Figure 12 is an overall model of Simulink. A block at the left is *USRP2 receiver* which masks a real USRP2 device and transmits samples in a frame of 358 samples in complex value to *SCF Analyzer*. Through the USRP2 receiver

block, center frequency, gain, decimation factor and output data type are controlled.

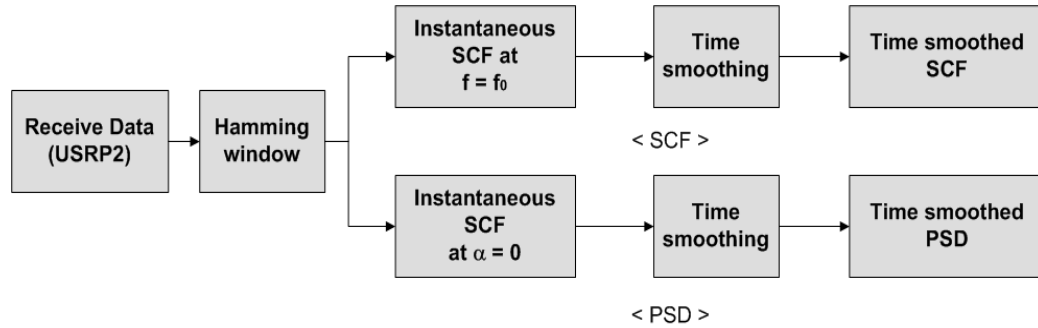


Figure 12. Simulink block model

The received samples go through the hamming window, and then its *instant SCF* is calculated using Equation (9). The *instant SCF* is analyzed both at particular frequency value, set to center frequency of signal, which is for SCF and at particular alpha value set to 0, which is for PSD.

The SCF values coming from the *instant SCF* are transferred to *Time smoothing* block which takes n sets of instantaneous SCF values and computes the mean of the n sets to get time-smoothed SCF values, which is characterized as a time smoothing degree, $\Delta t / T$ in Equation (13). The *Time smoothing* block outputs the time smoothed SCF values, plotting and recording them simultaneously.

- Validation
 - Validation of USRP2

The validation of correct working of USRP2 was done by comparing the PSD of the transmitted signal from USRP2 with that from spectrum analyzer. Two

things were investigated to validate the USRP2. First, a frequency offset was found in the USRP2, which occurs from USRP2 hardware itself estimated to be by thermal issue and to be different for each USRP2 and its decimation factor. This frequency offset was manually determined and manually compensated by specifying the center frequency as (*desired center frequency – frequency offset*). The frequency offset is shown below in Figure 13.

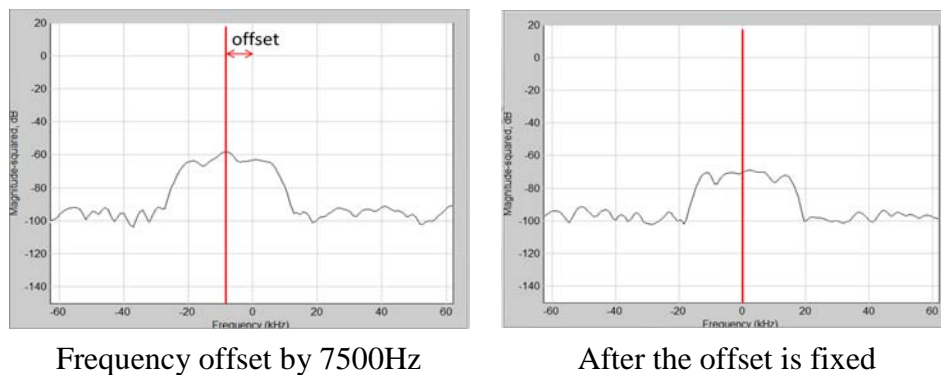


Figure 13. Frequency offset in USRP2

One more validation of USRP2 is the dB offset between Simulink and spectrum analyzer. The dB offset was found to non-exist in USRP2. The background noise is approximately a little bit lower than -90dB and the signal is -70 dB in both graphs in Figure 14. Width of the signal appeared to be same as 40 KHz knowing that each X-axis tick in both graph takes 20 KHz.

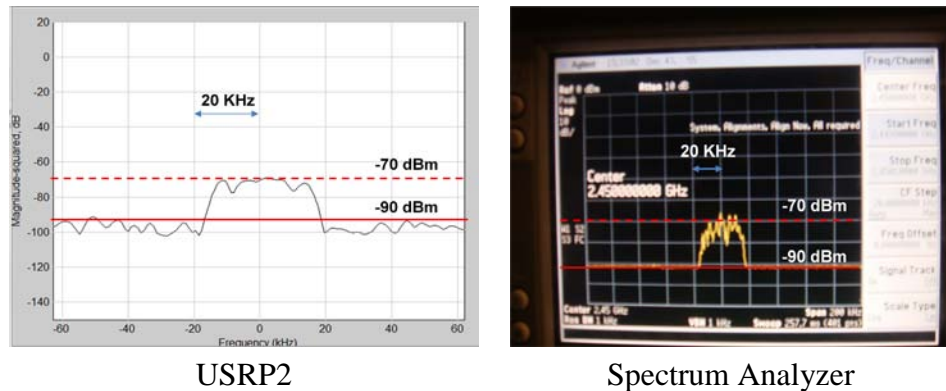


Figure 14. dB offset in USRP2 and Spectrum analyzer

A limitation of USRP2 for the research was found, which constraints the selection of modulation types. Signal features of negative frequency band and positive frequency band are identical. It is due to Digital Down Conversion (DDC) process built in Field Programmable Gate Arrays (FPGA) in USRP2. It prevents the SCF analyzer from getting correct SCF features resulting from multiplying frequency component of signal in positive frequency band by frequency component of signal in negative frequency band. Most of SCF features of many modulation types have such SCF features. That is, as seen in Figure 1, distinct SCF features of BPSK, QPSK, SQPSK signal are from multiplying spectral components of positive and negative frequency band. However, in Figure 2, some of distinct SCF features of 4-FSK signals are from multiplying spectral components only in one side of frequency band, because FSK modulation type has several distinct peaks only in one side of frequency band. Therefore, 2-FSK modulation type is chosen in the research, because 2-FSK signal is its own SCF features coming from only positive frequency band.

- Validation of computation

The validation of SCF computation used is done by comparing different computation approaches using real 2-FSK, BPSK and synthetic BPSK signal. Instead of looking at values at particular frequency and cycle frequency, whole SCF of the signals are investigated through a bi-frequency plane. Because of USRP2 hardware limitation, only positive frequency band is analyzed.

Computation approaches compared here can be divided to FFT based SCF (as shown in Equations (12) and (13)) and CAF based SCF (shown in Equation (4)). FFT based SCFs are further divided by time smoothing method, which are called *time windowing* and *time stepped* in this work. *Time windowing* is based on Equation (12) which takes T samples for every one time increment. *Time stepped* is based on Equation (13) which takes T samples for every T time increments.

Appendix B shows that FFT based SCF features with time-stepped time smoothing method (Appendix B (a)) has most distinct features. CAF based SCF features are blurrier than SCF based features. Between FFT based SCF features, time-stepped smoothing method has more distinct features with 2-FSK signal. From SCF features of BPSK, 2-FSK signals, it is show that SCF of individual positive frequency band has no SCF features other than when $\alpha = 0$, whereas 2-FSK has its unique SCF feature with its individual positive frequency band. Therefore, FFT based SCF with time-stepped smoothing is used in this experiments with 2-FSK signal.

3.11 Design of Experiments (DOE)

The experiment is to investigate SCF values at every configuration. The experiments are separated in three kinds of experiments. One is about changing environment - distance, location - which is done by full-factorial design. Another is about varying SNR levels and observation time with fixed distance and location. The last one is about observation time at a fixed distance and location. At least 30 replications are expected for a sufficient statistical basis for analysis [43]. Replication is done by one long measurement and dividing it to 40 sub- measurements based on regenerative simulation technique assuming all sub-measurements are independent and identically distributed [44].

The first experiment varying distance and location needs minimum measurements of:

$$\mathbf{15 \text{ (distance)}} \times \mathbf{8 \text{ (location)}} \times 1 \text{ (fixed transmit power)} \times \\ 3 \text{ (fixed observation time)} \times 1 \text{ (40 replications)} = 360$$

Next, Observation time is varied at each SNR levels. It requires, at a minimum, measurements of:

$$1 \text{ (fixed distance)} \times 1 \text{ (fixed location)} \times \mathbf{22 \text{ (transmit power)}} \times \\ \mathbf{4 \text{ (observation time)}} \times 1 \text{ (40 replications)} = 88$$

Lastly, observation time is varied to figure out effects of observation time on SCF features statistics

$$1 \text{ (fixed distance)} \times 1 \text{ (fixed location)} \times \mathbf{1 \text{ (transmit power)}} \times \\ \mathbf{7 \text{ (observation time)}} \times 1 \text{ (40 replications)} = 7$$

Therefore, a total of 455 measurements are required for the research.

3.12 Analysis

Given the results, analysis should be made to support the goals of the research.

For path loss experiments, analysis of path loss is based on “Log-normal shadowing” model for both indoor and outdoor experiments. Measured SCF are compared with measured PSD and robustness to noise is investigated by looking at its path loss exponents and variance.

For SNR and observation time experiments, measured SCF are compared with PSD in terms of noise floors by varying SNR. Noise floor which starts at lower SNR level can be said to be robust to noise. In addition, relation between observation time and noise tolerance is verified by looking at noise floors for each observation time.

Curve fitting for measured data is performed using Least Squares curve fitting method which minimizes deviation from all data points.

The effect of observation time is analyzed by looking at variance of SCF feature magnitude. Additionally, the variance of SCF feature is compared to the theoretic analysis of SCF.

3.13 Summary

This chapter talked about the system under test including component under test, services provided, system parameters and workloads. From the list of parameters and workloads, location, distance, signal power, observation times are the chosen factors. The performance metric is SCF value at a particular (f, α) coordinate where the distinct, highest peak exists in $\alpha \neq 0$ area. The full factorial design was chosen using real world measurements as an evaluation technique.

IV. Analysis and Results

4.1 Chapter Overview

The experiments are divided into the 3 separate parts described in Chapter III, including path loss analysis, SNR analysis, and observation time analysis. Results of path loss experiments are analyzed in Section 4.2.1 and results of SNR and observation experiments are analyzed in Section 4.2.2. In addition, the difference between synthetic AWGN and real world noise are statistically compared to complement the results.

4.2 Results

4.2.1 Path loss

Path loss experiments are executed at 8 different locations (as outlined in Chapter 3), varying distance between transmitter and receiver from 30 cm to 15 m. The SCF and PSD are investigated at the same time to compare their path loss under same conditions. The magnitude of the PSD and SCF features in all locations as well as separation distances are presented in dB scale. To see the effects of noise, the path loss exponent (which is slope of the magnitude-distance dB plot) and variance of the features are analyzed.

First, path loss trends are analyzed to see path loss exponents because path loss exponent reflects the effect of shadowing and multipath. In PSD, a path loss in dB domain is expected to increase linearly as distance in dB domain increases, which is same with linear decrease of signal strength magnitude in dB domain as distance in dB domain increases. And, at some point of distance, the signal strength stops decreasing and shows a steady state expected value (with certain strength from the distance as shown in [7]).

This behavior is also expected to happen with the SCF. The two states, which are the "path loss state" (decreasing value) and the "noise floor state" (steady value), are investigated by looking at the SCF / PSD feature value trends. Generally, transitions from the path loss state to noise floor happen smoothly as distances get longer. However, to analyze each state, the smooth trends are analyzed into one linear path loss trend and one constant noise floor trend. That is, each of the states is expected to have one straight line which reflects trend of each state. Path loss exponents are obtained from the slope of the linear path loss line. To fit measured data into the trend, Least Squares (LS) fit is used, as described in [7].

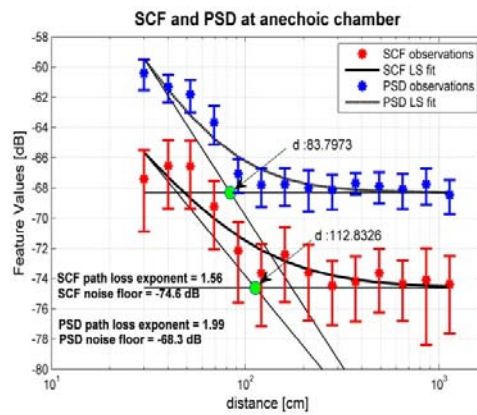
Second, variances of the SCF / PSD measurements are obtained by averaging variances of measurements except the measurements on noise floor for every observation times and compared. The reason why variance of the SCF / PSD is investigated is that it reflects small fluctuations which are mainly due to multipath (fast fading).

Additionally, during the experiments, observation times are varied in 3 different levels (512, 8192, 131072 samples) to see effects of observation time on path loss by looking at path loss exponents at each observation time. Path loss exponents at each observation time are presented with Root Mean Squared Error (RMSE) of the LS fit to capture whether the LS fit of path loss is comparatively accurate or not. For path loss plots, results at 8192-sample observation time are used.

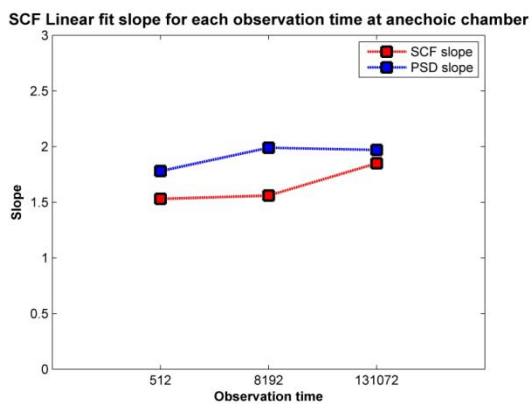
4.2.1.1 Anechoic chamber

The first location investigated is the anechoic chamber. The anechoic chamber is a room where reflection is minimized as well as external interference and noise. Thus, it

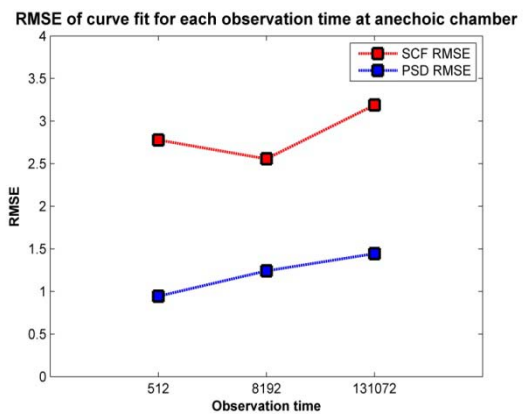
can be considered as a quiet open space. Since it has been designed to have the least amount of noise and reflections, results from this location will be thought of as the “standard” of the path loss experiments. That is, results from other locations will be compared to the results from this anechoic chamber not for comparing overall performance in certain area, but for comparing effects of noise such as multipath and shadowing. Due to the size of the anechoic chamber, 14 measurements are taken instead of 15 measurements.



(a) SCF / PSD path loss



(b) Fit curve slopes



(c) RMSE

Figure 15. Anechoic chamber

In the anechoic chamber, the SCF path loss exponent was smaller than the PSD path loss exponent by 0.43 as can be seen in Figure 15 (a). This could mean that in the environment like the anechoic chamber with almost no multipath and no shadowing, the SCF has more distinct features than the PSD. That is, the SCF features can be said to be more robust at the lower SNR induced by distance path loss than the PSD. Since multipath is minimized in this environment, this does not provide any evidence that the SCF is more robust to other noise effects such as multipath and shadowing. Figure 15 (b) and (c) showed that for every length of observation time, the SCF had a lower path loss exponent than the PSD. In terms of the effect of observation time on SCF / PSD, as observation time increased, the path loss exponents of the SCF and PSD tended to increase by only 0.3 and 0.2. In addition, the large RMSE of fit doesn't seem to support that these differences between each observation times are significant.

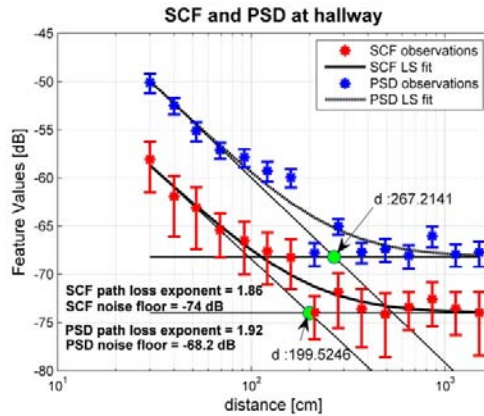
The variance of the SCF is smaller than that of the PSD at every observation times as in Table 4. It can be said that without any multipath and shadowing the SCF showed less variance than the PSD.

Table 4. Variance of SCF / PSD at each observation time in anechoic chamber

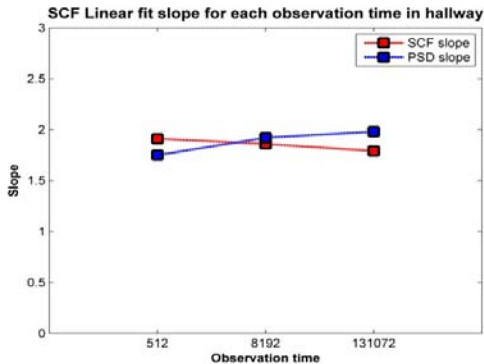
Observation time	SCF (dB)	PSD (dB)
512 samples	-128.1335	-125.6733
8192 samples	-142.0570	-137.2534
131072 samples	-153.0965	-147.1524

4.2.1.2 Hallway

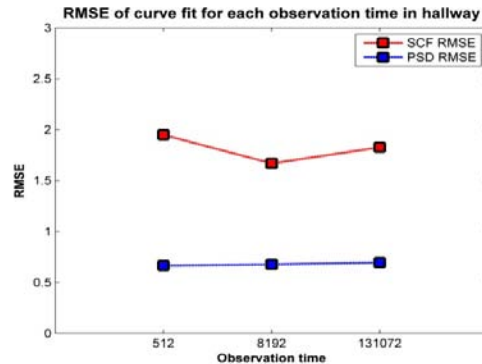
The hallway can be thought of belonging to an indoor LOS environment with strong multipath components. Measurements were taken with a transmitter fixed and a receiver moving for each distance as in Figure 16 (d) and (e).



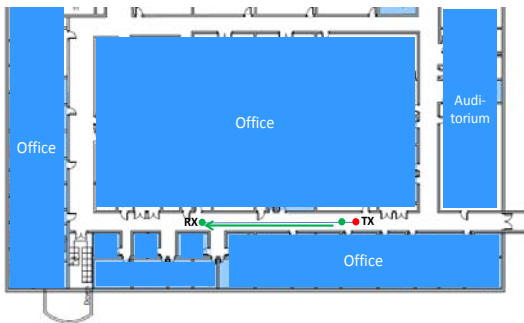
(a) SCF / PSD path loss



(b) Fit curve slopes



(c) RMSE



(d) Floor plan



(e) Hall way

Figure 16. Hallway

In a hallway with LOS, the SCF path loss exponent was smaller than the PSD path loss exponent by 0.06 in Figure 16 (a). But the SCF and the PSD showed similar performance, in terms of overall noise effects such as distance dependent path loss, multipath, shadowing, because the 0.06 difference in the path loss exponents is small when considering the large RMSE as in Figure 16 (c). However, when compared to the results of anechoic chamber, the path loss exponent of the SCF increased by 0.3 while the path loss exponent of the PSD decreased by only 0.07. This could mean that in the environment like the hallway with multipath, the SCF is not as robust to multipath as the PSD is. In addition, Figure 16 (b) doesn't show any significant changes in path loss exponents as observation time changes.

The variance of the SCF was smaller than the PSD for every observation times, as shown in Table 5.

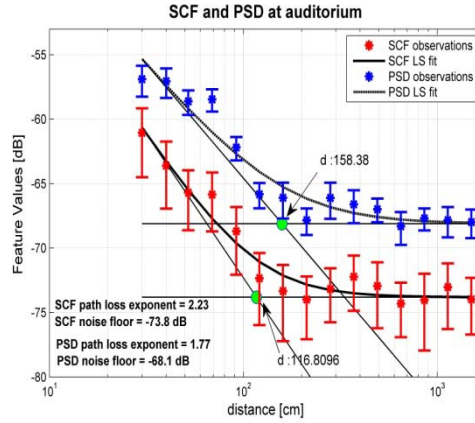
Table 5. Variance of SCF / PSD at each observation time at hallway

Observation time	SCF (dB)	PSD (dB)
512 samples	-116.383	-111.024
8192 samples	-128.861	-120.41
131072 samples	-140.969	-128.861

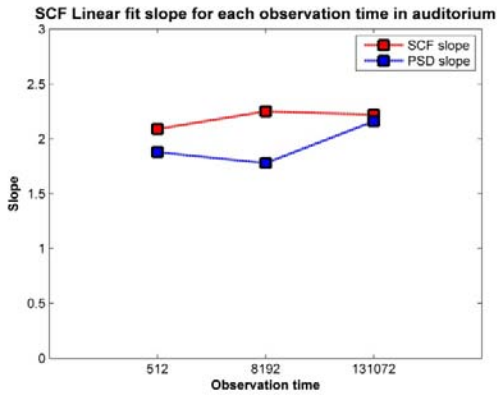
4.2.1.3 Auditorium

The auditorium can also be thought of as an indoor LOS environment like the hallway above. The differences between them are the distances to walls and that there's no way of transmitted signal to get out. That is, every signal is reflected through walls surrounded until their strength weakens. It is expected that the longer distance from the receiver and transmitter to walls can reduce multipath effects, whereas the fact that all direction are

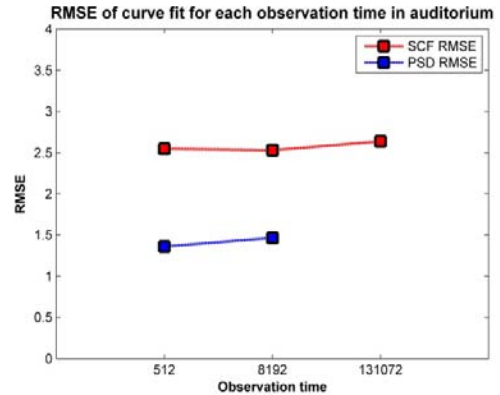
surrounded can result in more multipath effects. Results of the experiment are shown below in Figure 17.



(a) SCF / PSD path loss



(b) Fit curve slopes



(c) RMSE



(d) Auditorium

Figure 17. Auditorium

In auditorium, the SCF path loss exponent was larger than the PSD path loss exponent by 0.46 in Figure 17 (a). Overall, the SCF showed worse performance than the PSD when simply comparing the path loss exponents of them. When compared to the SCF path loss exponents in anechoic chamber, the SCF path loss exponent increased by 0.67 in the auditorium, while the PSD path loss exponent decreased by 0.22. This could indicate that, in the environments like the auditorium, SCF is not more robust to multipath and shadowing than PSD. Thus, it can be said that the SCF was more affected by multipath and shadowing than the PSD in this location. This higher path loss exponent kept same for every observation time. And, as same with previous results, observation time doesn't seem to have effects on path loss exponents because while varying observation time, the path loss exponents kept similar considering larger RMSE in Figure 17 (b) and (c). The RMSE of observation time 131072 was not generated because the degree of freedom was too small to obtain it.

From the Table 6, it is shown that the SCF variances at every observation time are smaller than the PSD, keeping the consistency as observation time varies.

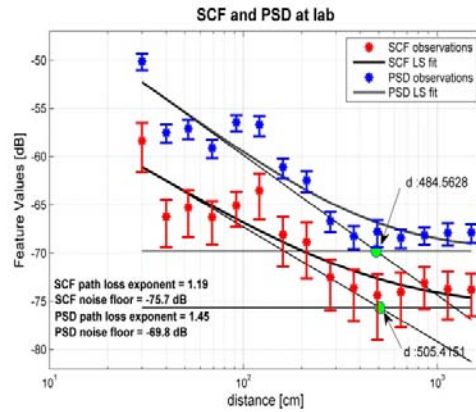
Table 6. Variance of SCF / PSD at each observation time at Auditorium

Observation time	SCF(dB)	PSD(dB)
512 samples	-122.518	-118.239
8192 samples	-133.979	-129.586
131072 samples	-146.778	-132.147

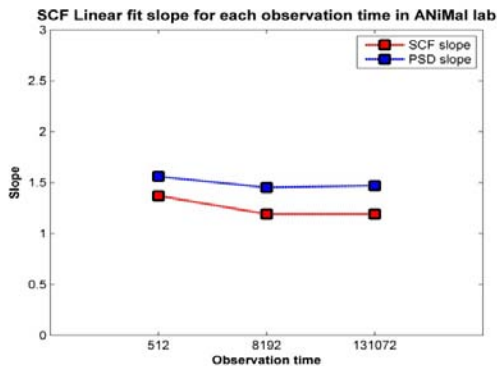
4.2.1.4 ANiMaL Lab

ANiMaL lab was chosen to model "obstructed in factories" environment as in Table 3. LOS is not guaranteed as in Figure 18 (d). Between a receiver and a transmitter, there

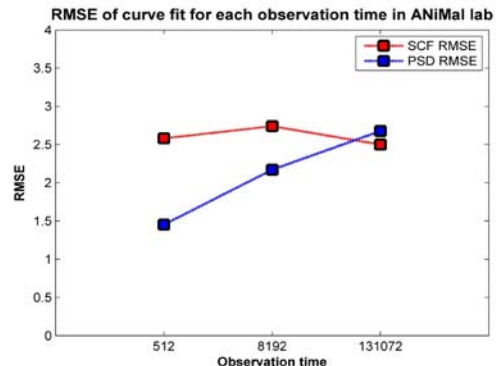
are a thin wall and other obstructions such as desks. And up to a certain point of distance, an obstruction between transmitter and receiver is same, which is just a thin wall. But from the certain point of distance, obstructions between them increased, as seen in Figure 18 (e).



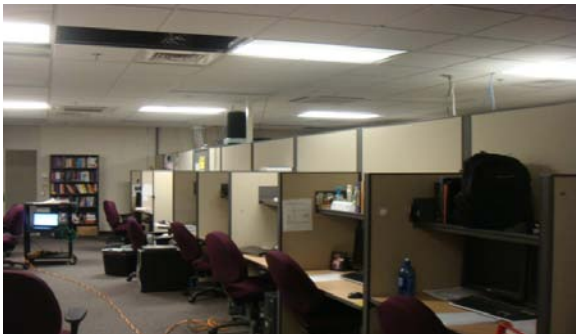
(a) SCF / PSD path loss



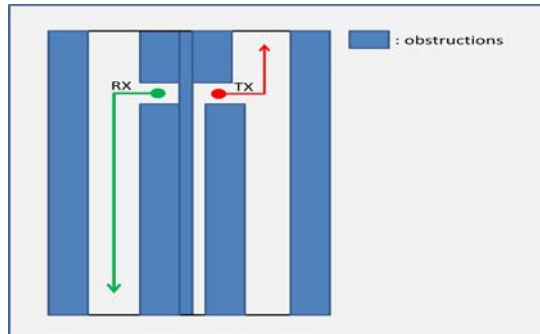
(b) Fit curve slopes



(c) RMSE



(d) ANiMaL Lab



(e) Floor Plan

Figure 18. ANiMaL Lab

In the lab without LOS, the SCF path loss exponent was smaller than the PSD path loss exponent 0.26 as in Figure 18 (a). That is, overall, the SCF showed better performance than the PSD. When compared to the results of anechoic chamber, both the SCF and the PSD had smaller path loss exponent than those in anechoic chamber. The SCF decreased by 0.37 and the PSD decreased by 0.54. It is estimated that the reason why the path loss exponent decreased is that multipath has not only destructive effects but also constructive effects and, in the lab, the constructive effects affected more than the destructive effects. The PSD seems to have more constructive effects than the SCF. Thus, it could mean that in the environment like ANiMaL lab the SCF is more robust to multipath and shadowing effects because the PSD path loss exponent decreased more. From the Figure 18 (b), even though observation time doesn't seem to have effects on the path loss exponent as previous, smaller SCF path loss exponents are observed at every observation time (consistently).

In the Table 7, variances of the SCF were smaller than the PSD for all observation times, still maintaining the consistency.

Table 7. Variance of SCF / PSD at each observation time at ANiMaL Lab

Observation time	SCF(dB)	PSD(dB)
512 samples	-118.861	-111.367
8192 samples	-131.805	-123.768
131072 samples	-143.768	-136.021

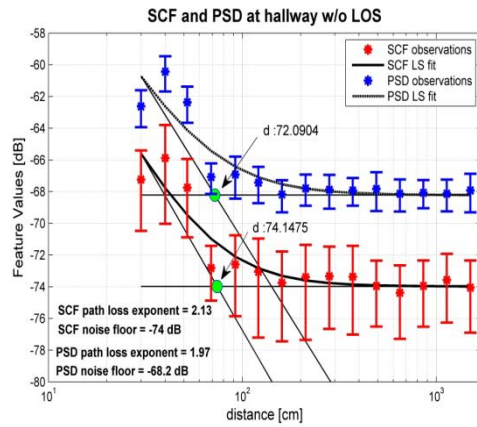
In short, in the environment like the ANiMaL lab, both the SCF and the PSD seemed to have constructive multipath effects and the PSD was more affected by the effects based on the change of the path loss exponents when compared to the anechoic chamber

case. Variances at every observation time also support that the SCF had less multipath effects based on smaller variance, keeping consistency.

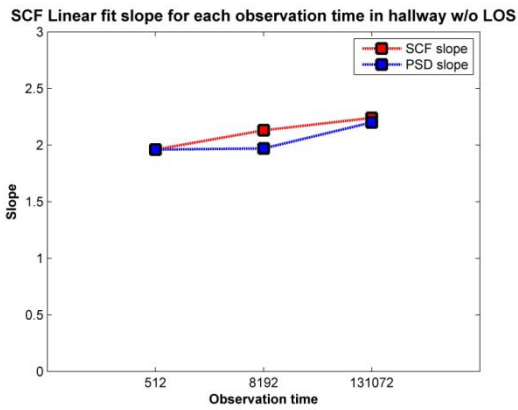
4.2.1.5 Hallway without LOS

This environment was chosen to model "obstructed in building" environments. Obstructions here are thicker / denser obstructions than previous experiment at the lab. Because the LOS is not guaranteed, shadowing is expected to affect the path loss more than in LOS-guaranteed cases. But, there still are multipath effects as well. Difference of obstruction between this location and ANiMaL lab is how dense the obstructions are. In this case, the obstruction was a concrete wall which is dense, whereas in ANiMaL lab, the obstruction was a cubicle wall which is sparse. A transmitter and a receiver were set as Figure 19 (e) and the receiver moved as Figure 19 (d).

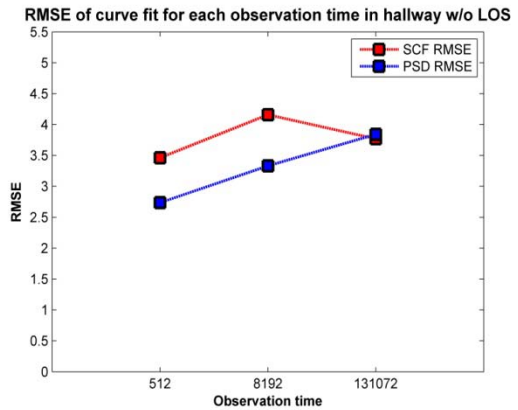
In a hallway without LOS, the SCF path loss exponent was larger than the PSD path loss exponent by 0.16 in Figure 19 (a). That is, overall, the SCF showed a little worse performance than the PSD. When compared to the results of anechoic chamber, the SCF increased by 0.57 and the PSD decreased only by 0.02. The decrease of the PSD is negligible considering the large RSME in Figure 19 (c). This indicates that the SCF was more affected by multipath and shadowing than the PSD in this location. Figure 19 (b) shows that there were no significant path loss exponent changes as observation time changes.



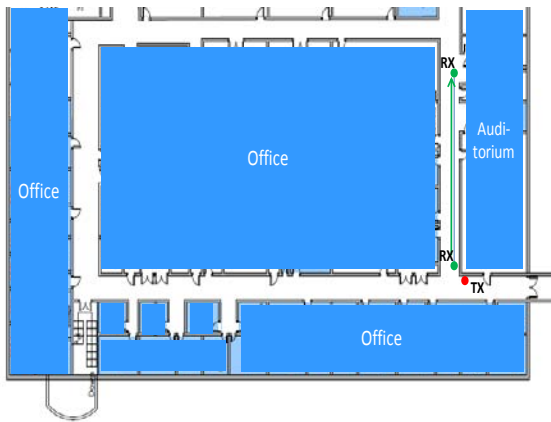
(a) SCF / PSD path loss



(b) Fit curve slopes



(c) RMSE



(d) Floor plan



(e) Hall way

Figure 19. Hallway without LOS

In Table 8, variances of the SCF are smaller than that of the PSD at observation times, maintaining consistency of path loss exponent as observation time varies.

Table 8. Variance of SCF / PSD at each observation time at Hallway without LOS

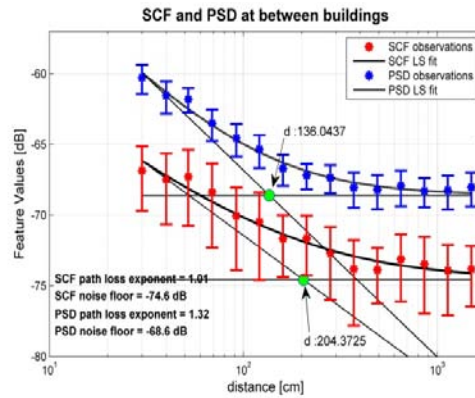
Observation time	SCF(dB)	PSD(dB)
512 samples	-127.696	-125.376
8192 samples	-141.308	-137.696
131072 samples	-152.84	-144.202

Experiments at indoor environments were considered so far. Indoor environments have more possibilities to have more multipath effects than outdoor environments, because signals can be reflected back to a receiver even though the signal wave already passed by. It can be good or bad for a receiver because such multipath can have constructive and destructive effects on received signal.

From now on, experiments are executed in outdoor environments. Outdoor environments don't have ceilings that transmitted signal waves propagated towards upside are not reflected back to receiver. Only objects on path between or near a receiver and transmitter contribute to the noise effects.

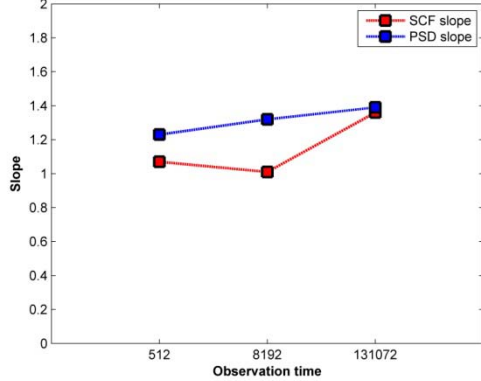
4.2.1.6 In between buildings

This place was chosen to model "urban area" with buildings around and LOS guaranteed. As seen in Figure 20 (d), there are buildings around a transmitter and a receiver.



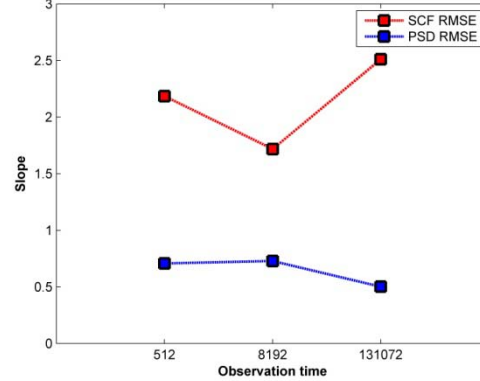
(a) SCF / PSD path loss

SCF Linear fit slope for each observation time at between buildings



(b) Fit curve slopes

RMSE of curve fit for each observation time at between buildings



(c) RMSE



(d) Between building with LOS

Figure 20. In between buildings

In between buildings, the SCF path loss exponent was smaller than the PSD path loss exponent by 0.31 as in Figure 20 (a). That is, overall, the SCF showed better performance

by simply comparing the path loss exponent of the SCF and the PSD. When compared to the results of anechoic chamber, the path loss exponent of the SCF decreased by 0.55 and the PSD decreased 0.67. Constructive multipath effects also seem to take place in this environment because the path loss exponents decreased in both SCF and PSD. In the decreases, PSD showed a little more decrease than the SCF by 0.12, which indicates that the PSD was a little more affected by the constructive multipath effects. Observation time doesn't seem to affect the path loss exponents of SCF and PSD. The SCF maintains slightly smaller path loss exponents than the PSD for every observation times as in Figure 20 (b).

In Table 9, the variances of the SCF are smaller than that of the PSD for all observation times, keeping consistency with previous results.

Table 9. Variance of SCF / PSD at each observation time at between buildings

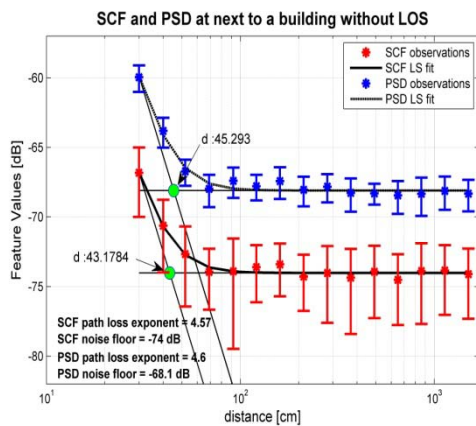
Observation time	SCF(dB)	PSD(dB)
512 samples	-128.861	-126.576
8192 samples	-143.372	-137.959
131072 samples	-154.437	-148.239

4.2.1.7 Next to a Building without LOS

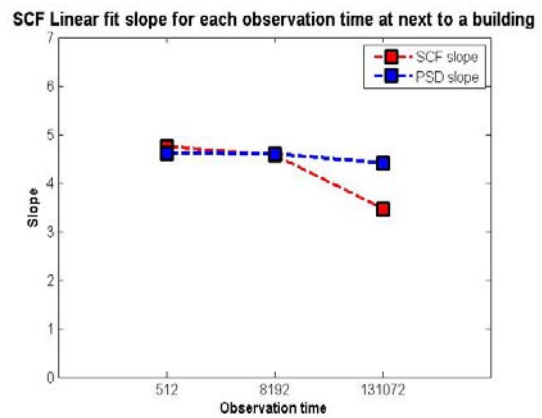
This place was chosen to model "shadowed urban area" with buildings around and LOS not guaranteed as in Figure 21(c). In this case, shadowing is expected to affect the path loss more than LOS guaranteed cases.

At next to a building, the SCF path loss exponent was a little smaller than the PSD path loss exponent by 0.03 as in Figure 21 (a). That is, overall, the SCF and the PSD showed similar performance because the 0.03 difference in the path loss exponents is

small when considering large path loss exponents in Figure 21 (b). When compared to the results of anechoic chamber, the path loss exponent of the SCF increased by 3.01 and the PSD increased by 2.61. The SCF seems to have more noise effect than the PSD in this location. In Figure 21 (b), path loss exponents of the SCF and the PSD are not similar for all observation times. (inconsistency) RMSE was not generated because degree of freedom was too small to obtain it.



(a) SCF / PSD path loss



(b) Fit curve slopes



(c) Next to the building without LOS

Figure 21. Next to building without LOS

In the Table 10, it shows that, for every observation times, the SCF showed smaller variance than the PSD, keeping consistency with previous results.

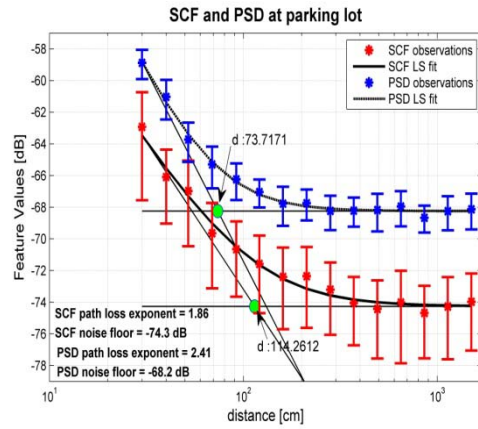
Table 10. Variance of SCF / PSD at each observation time next to building

Observation time	SCF(dB)	PSD(dB)
512 samples	-134.685	-131.079
8192 samples	-150	-144.949
131072 samples	-162.441	-155.686

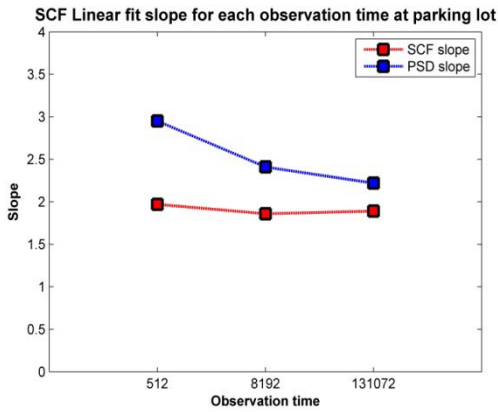
4.2.1.8 Parking lot

This place is close to "free space" with nothing around and LOS guaranteed as in Figure 22(d). In other words, this place is expected to have little multipath and shadowing effects compared to other environments above except the anechoic chamber. However, there still exist unexpected objects such as lights, trees and so on. And this place is not expected to have as little noise effects as the anechoic chamber.

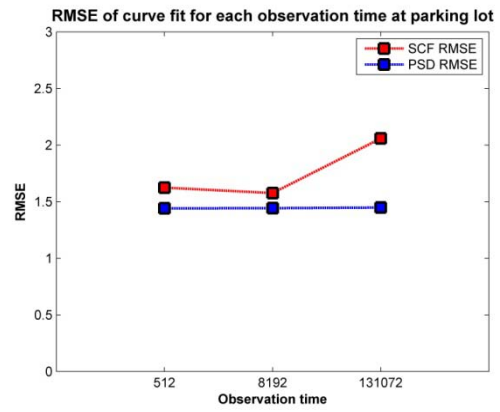
At parking lot, the SCF path loss exponent was smaller than the PSD path loss exponent by 0.55 as in Figure 22 (a). That is, overall, the SCF showed better performance than the PSD. When compared to the results of anechoic chamber, the path loss exponent of the SCF increased by 0.3 and the PSD increased by 0.42. And for every observation times, the SCF keeps less steep path loss exponents than the PSD as in Figure 22 (b).



(a) SCF / PSD path loss



(b) Fit curve slopes



(c) RMSE



(d) Parking Lot

Figure 22. Parking lot

In the Table 11, it shows that, for all observation times, the PSD had smaller variances than the SCF, maintaining consistency with previous results.

Table 11. Variance of SCF / PSD at each observation time at Parking Lot

Observation time	SCF(dB)	PSD(dB)
512 samples	-125.528	-124.559
8192 samples	-137.959	-136.778
131072 samples	-152.291	-151.308

4.2.1.9 Short Conclusions

At 8 locations, measurements were taken varying distances in 15 levels. Path loss exponents of SCF / PSD path loss and variances of SCF / PSD feature values are investigated and overall results are shown in Table 12.

Table 12. Path loss exponents in each locations / path loss exponent differences to anechoic chamber / variance

		Anechoic chamber	Hallway	Auditorium	Lab	Hallway w/o LOS	Between buildings	Next to building	Parking lot
Path loss exponent	SCF	1.56	1.86	2.23	1.19	2.13	1.01	4.57	1.86
	PSD	1.99	1.92	1.77	1.45	1.97	1.32	4.6	2.41
Path loss exponent difference	SCF	.	0.3	0.67	-0.37	0.57	-0.55	3.01	0.3
	PSD	.	-0.07	-0.22	-0.54	-0.02	-0.67	2.61	0.42
Smaller Variance	SCF	SCF	SCF	SCF	SCF	SCF	SCF	SCF	SCF

Table 12 shows path loss exponents of the SCF / PSD path loss at each locations and path loss exponent differences between at anechoic chamber and at each location. Path loss exponents at each location may reflect performances of SCF / PSD at each location. Because the performance can be different from robustness to noise effects, therefore, path loss exponent differences are investigated, which possibly reflect the robustness to noise effects.

Positive values in the difference mean increase of path loss exponent and negative values mean decrease of path loss exponent. But, since we only look at magnitude of the differences as a result of noise effect, whether it is a positive value or a negative value doesn't matter. Blue-colored cells in the table indicate smaller value when comparing between the values at the SCF and the PSD.

At 5 out of 7 locations (except anechoic chamber), the SCF showed smaller path loss exponents which could indicate that, in these 5 places, the SCF showed better performance. However, in terms of robustness to noise effects, only at 3 places out of 7, the SCF showed smaller differences, which could indicate that more robustness to noise effects. That is, because the path loss exponent differences of the SCF are not consistently smaller than that of the PSD, it is hard to say that SCF is more robust to PSD in general.

However, in terms of variance at each location, the SCF exhibited smaller values than the PSD consistently, which could indicate robustness of SCF to noise effects, especially multipath.

4.2.2 SNR and Observation time

In this section, the performance of SCF over PSD is verified against real world signals and background noise by varying the SNR for each observation time to compare against Figure 8 which showed that noise floor of SCF appear in lower SNR environments than that of PSD and as observation time gets longer, noise floor also appear in lower environments than the noise floor with shorter observation time. In

addition, by varying the observation time, its effect on the SCF feature is inspected and compared with the theoretical statistics discussed with Table 2 in Section 2.5.

4.2.2.1 SNR with observation time

First, the SNR was varied by controlling the transmit power of signal. The receiver analyzed the collected signal in terms of the SCF and PSD. In addition, the observation time was varied in 4 different levels. Results of these experiments are compared to Figure 8 which is generated by the simulation. Figure 23 below shows results of our experiments of varying SNR with different observation times.

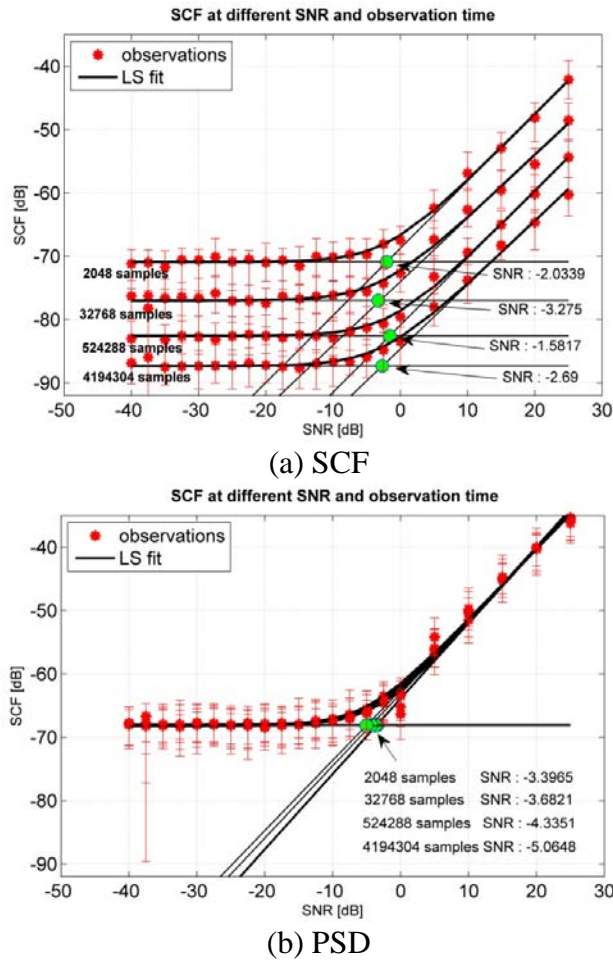


Figure 23. SCF vs. PSD with varying SNR and observation time

Figure 23 (a) shows SCF feature values of the experiments. For $\text{SNR} > 0$ dB, the feature value decreases linearly in dB scale as SNR goes to 0 dB. From a certain point of SNR, the feature values are almost the same values, showing no more decrease or increase in values, which is the noise floor. The trends of feature values seem to be same with the Figure 8 in the way that it has a linear decreasing line and a noise floor.

However, in terms of observation time, it is shown that the observation time doesn't affect the position of starting point of SCF floor (green circles in the figure). That is, the noise floors of SCF features from every observation time start at almost same SNR level. This is different from what is seen in Figure 8, because, in Figure 8, as observation time gets longer, the starting point of the noise floor shows up at lower SNR levels. The observation time also decreases the SCF value both in high and low SNR environments. This result is also different from Figure 8 in Section 2.5, which showed the same SCF features for different observation time under high SNR environment. This even more surprising because the PSD feature in Figure 23 (b) shows the almost same starting point position of PSD floor with that of SCF floor starting point in Figure 23 (a). These results do not provide evidence that the show that the SCF outperforms the PSD. In conclusion, with real world signal and background noise, it appears that the SCF does not have better performance than the PSD and does not show a distinct feature in low SNR environment. Rather the features diminish as SNR gets lower.

4.2.2.2 Observation time

In the previous Section 4.2.2.1, the effect of observation time was introduced under the factor of varying the SNR, which decreased both the magnitude of the SCF feature as

well as the magnitude of the SCF noise floor. The result was compared with the simulation based result of observation time.

In addition, variance of SCF feature magnitude is also affected by observation time. As can be seen in Table 2, the statistical properties of the time smoothed SCF and PSD, especially the variance of the time smoothed feature, depend on the observation time. Using one of those properties, the effect of observation time is investigated. The real part of SCF feature of the signal with background noise ($\overline{re\{S_{x+c}^\alpha(k)\}}$) is used for this analysis.

The Figure 24 below shows the $\overline{re\{S_{x+c}^\alpha(k)\}}$ of a 2-FSK modulated signal with real world noise for each observation times. The red square denotes the mean of the feature and the lines denote the standard deviation.

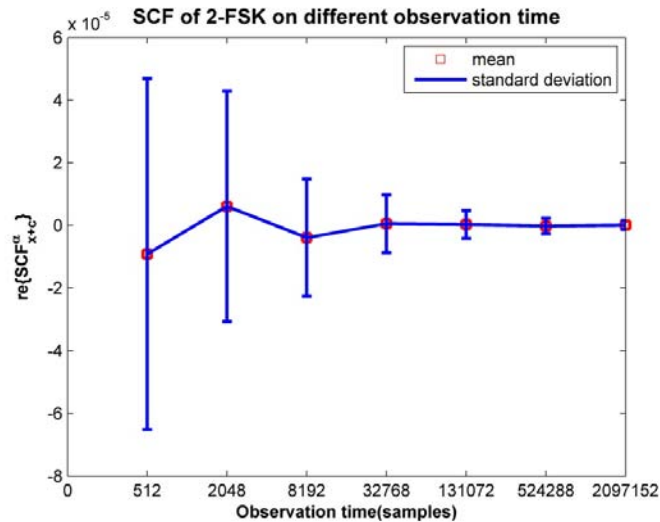


Figure 24. SCF of 2-FSK on different observation time

Theoretically with AWGN, $\overline{re\{S_{x+c}^\alpha(k)\}}$ variance should decrease as the observation time gets longer. The change in variance should follow N / T , as in Table 2. Figure 25

shows the variance of $\overline{re\{S_{x+c}^\alpha(k)\}}$ as observation time gets longer with real world noise.

A numerical description of the variance is described in Table 13 .

Table 13. Variance ratios of theoretical and experimental $\overline{re\{S_{x+c}^\alpha(k)\}}$

T (Observation time)	512	2047	8192	32768	131072	524288	2097152
N (FFT resolution)	-----		512	-----			
N / T	1	0.25	0.0625	0.01563	0.00391	0.00098	0.00024
Ratio of theoretical variance	1	0.25	0.0625	0.01563	0.00391	0.00098	0.00024
Variance ($\times 10^{-8}$) from experiment	0.3138	0.1353	0.0350	0.0086	0.0020	0.0006	0.0002
Experimental ratio of variance	1	0.4312	0.1116	0.0273	0.0064	0.0020	0.0007

The variance of $\overline{re\{S_{x+c}^\alpha(k)\}}$ with real world signal and noise is shown in the 5th row of the table. From these values, ratios of the variance are obtained and it shows that whereas although the analysis shows that when the observation time is quadrupled, the variance should reduce by a factor of 1/4, the experimental ratio shows a factor of 1/2.3 ~ 1/4.3, which reflects the theoretical ratio. In conclusion, observation time affects the variance of SCF feature and as the observation time gets longer, the variance diminishes. Numerically, the effect of observation time on the variance of SCF feature value can be said to follows the theoretical analysis in [12].

4.2.3 Difference between AWGN and real world noise

The SCF features with real world data did not show the same characteristics that the SCF theoretically should show. Specifically, the SCF with real world data exhibit little or no performance superiority of the PSD under low SNR environment and did not show distinct robustness to noise effects. One of the reasons why it showed no better performance under low SNR environment is that background noise of real world is not AWGN (which is independent, uncorrelated and Gaussian distributed). That is, real world noise can be dependent, correlated and/or not Gaussian distributed.

Here, the distributions of real world noise and AWGN noise (synthetic) are inspected in terms of its noise itself and its SCF.

First, using raw noise signal itself, Quantile-Quantile Plot (QQ Plot) is made to compare a distribution of synthetic AWGN and real world observed noise to normal distribution.

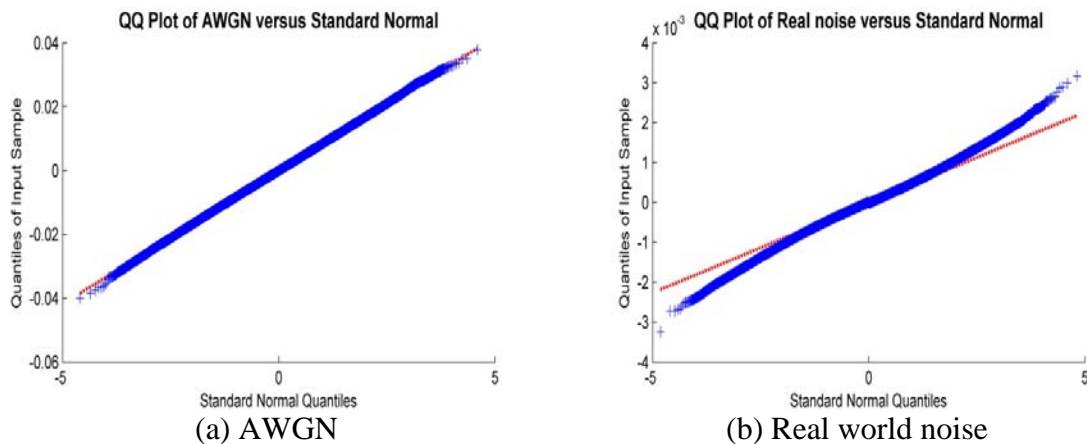


Figure 25. QQ Plot of AWGN and Real world noise

Figure 25 (a) is QQ plot of synthetically generated AWGN noise. It follows almost perfectly the red straight line, which indicates that the AWGN is normal distributed. However, Figure 25 (b), the QQ plot of real world noise, exhibits departures from the red

straight line (fitted line) in the tails. Thus, the real noise can be said not to be normal distributed. Rather, it is estimated from the Figure 25 (b) that it has long tailed distribution, because the middle of the data tends to be mild S-like shape pattern and first few points and last few points show departures from fitted straight line. To be specific, the QQ plot of the real world noise has increasing departures of first few points from the straight line below the line and also increasing departures of last few points from the straight line above the line, which indicates that the distribution has long tails [45].

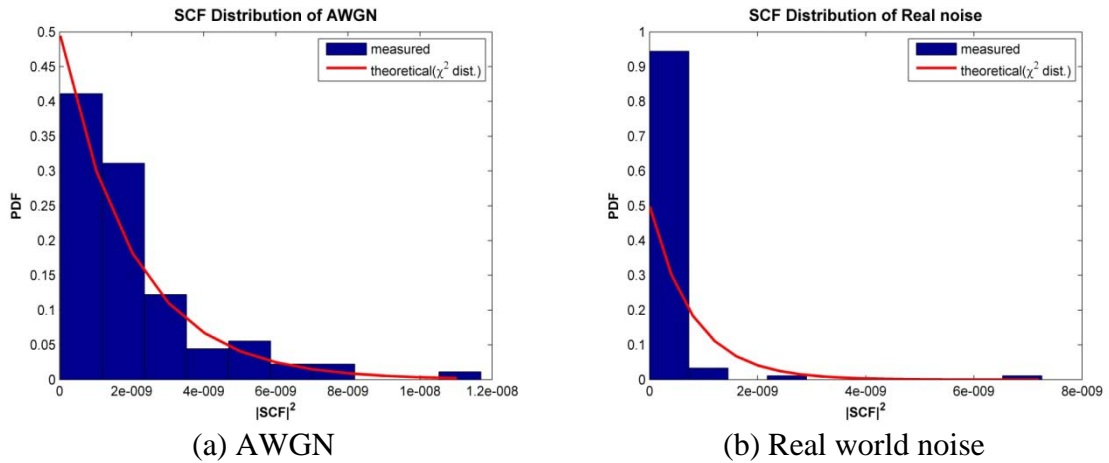


Figure 26. SCF Distribution of AWGN and Real world noise

The effect of this non-AWGN noise on the SCF is investigated by looking at the distribution of SCF under real world noise and versus under AWGN noise by plotting the SCF feature distribution as a histogram. Theoretically, if the noise was AWGN, the squared magnitude of the SCF ($|\overline{S_c^\alpha(k)}|^2$) under AWGN noise is expected to be chi-squared (see Table 2). Therefore, if $|\overline{S_c^\alpha(k)}|^2$ is not chi-distributed this implies that the real world noise is not Gaussian distributed.

4.3 Summary

Path losses measurements under SCF were obtained from several locations and compared with that of the PSD to see effects of noise caused by shadowing and multipath on the path loss exponent and feature variance. In terms of the path loss exponent, the SCF exhibited unclear robustness to noise effects over the PSD. However, in terms of variance, the SCF exhibited better robustness than the PSD. Outperformance of SCF over PSD under low SNR environments was not identified with real world modulated signal and back ground noise. The SCF features showed almost same performance in terms of SNR, which means that at almost same SNR level, the SCF and PSD feature disappeared into the noise floor. Also, even though observation time was supposed to make SCF outperform under low SNR environment with lowering the SNR level of starting point of feature floor, it didn't work as it was expected. Rather, observation time lowered all the feature values, not only features of noise but also features of signal. Statistics of SCF features were identified in terms of observation time and resulted in exhibiting similar feature shown by theoretical approach. Lastly, one of the reason why SCF didn't work as it was expected because the real world noise turned out to be different than AWGN.

V. Conclusions and Recommendations

5.1 Overview

This research has identified cyclostationary features of digitally modulated signals through empirical measurements using features of the spectral correlation function. This chapter summarizes the objectives and conclusions, discusses contributions to the field of study, and proposes future works.

5.2 Conclusions

5.2.1 Path loss of SCF

To identify and characterize cyclostationary features of modulated signals under channel noise and path loss, the magnitude of the SCF features were obtained from many locations and compared to those from the PSD. The path loss exponent and variances of the SCF features were investigated. It was found that, from the path loss exponents, that it is inconclusive whether the SCF features are more robust to noise effects than the PSD features. However, from the feature variances, it was found that the SCF does tend to be more robust to noise effect, especially multipath, because it has smaller variance than the PSD features.

5.2.2 SNR performance

To determine the difference in performance between the SCF over the PSD under a low SNR environment with real world signals, the SCF / PSD features were measured under varying SNR levels with different observation times. It was found that, under real world noise, SCF didn't show any outperformance under low SNR environment over

PSD, and additionally observation also didn't improve the outperformance of SCF over PSD under low SNR environments.

5.2.3 Effects of Observation time on the SCF statistics

To observe the effect of observation time on the SCF statistics, variance of real part of SCF feature of the signal with real world background noise ($\overline{re\{S_{x+c}^\alpha(k)\}}$) was investigated and compared to theoretical variance. It was found that the variance from real world experiments exhibited similar feature ratio shown by the theoretical approach in respect of observation time.

5.2.4 Difference between real world noise and AWGN

Because no distinct performance superiority of the SCF features over the PSD feature was found in this work, the difference between real world noise and AWGN was investigated. It was found that the real world noise does not follow a Gaussian distribution as the AWGN does. In addition, the statistics of the SCF feature under real world noise was investigated and it was found that there exists a discrepancy between these and those under AWGN.

5.3 Contributions

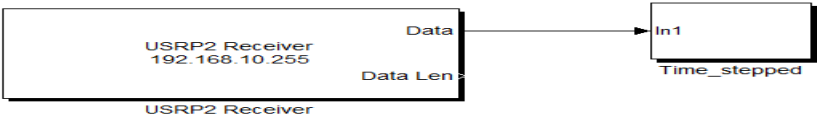
Through this work, we identified cyclostationary characteristics with real world signal under real world noise and examined the performance of SCF under real world noise. In addition, this work is expected to establish grounds for choosing signal detection method. Based on the results, CFD does not appear to be better than energy detection, because outperformance of the SCF was not proven with real world signal and

the CFD requires more information and more computations. And by showing AWGN is different from real world noise, importance of experimenting with real world noise is emphasized.

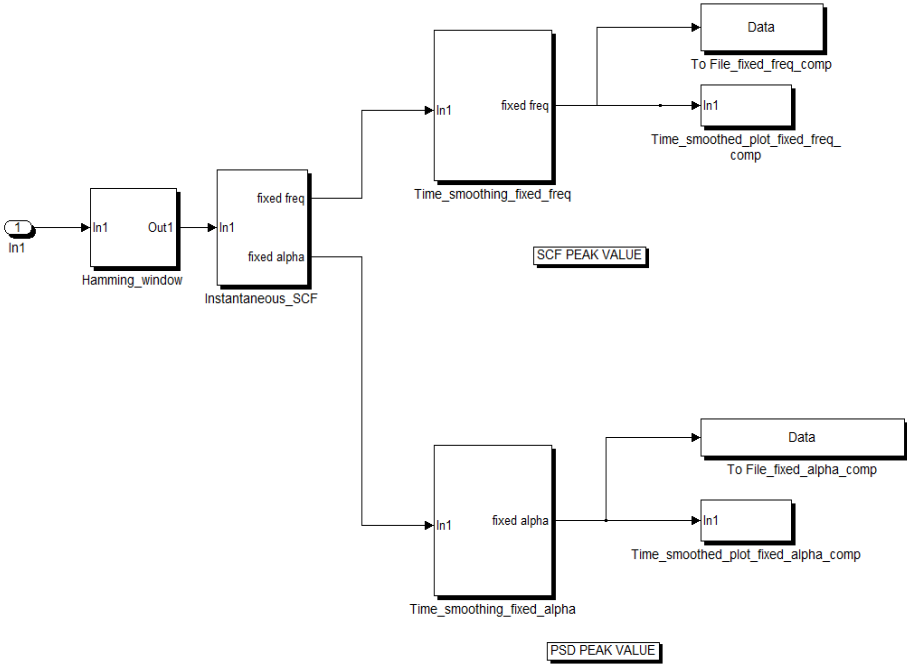
5.4 Future Work

Since we have not seen distinct improvements of SCF performance, changes in parameters used in this work would give more distinct features of the SCF. Finer frequency resolution is expected to distribute noise components over more frequency bins, which would make SCF feature more distinct. Therefore, experimenting and examining SCF performance with larger FFT resolution is suggested

Appendix A : Simulink model



(a) Overall Simulink Test Bed



(b) SCF Analyzer

Figure 27. Simulink block sets

The Simulink blocks in Figure 27 above describe how the data flows are analyzed. Figure 27(a) is an overall model of Simulink. A block at the left is *USR2 receiver* which masks a real USRP2 device and transmits samples in a frame of 358 samples in complex value to *SCF Analyzer*. Through the USRP2 receiver block, center frequency, gain, decimation factor and output data type are controlled.

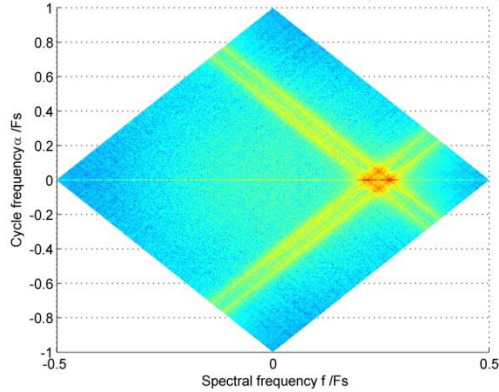
Figure 27(b) is detailed blocks of *SCF analyzer*. Received samples go through the hamming window, and then its *instant SCF* is calculated using Equation (9). The *instant*

SCF is analyzed both at particular frequency value, set to center frequency of signal, which is for SCF and at particular alpha value set to 0, which is for PSD.

The SCF values coming from the *instant SCF* are transferred to *Time smoothing* block which takes n sets of instantaneous SCF values and computes the mean of the n sets to get time-smoothed SCF values, which is characterized as a time smoothing degree, $\Delta t / T$ in Equation (13). The *Time smoothing* block outputs the time smoothed SCF values, plotting and recording them simultaneously.

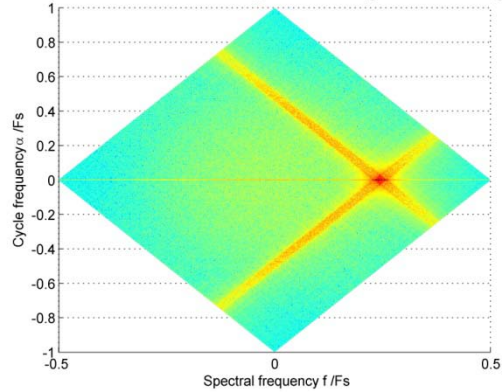
Appendix B : Different computational approaches of SCF

FFT based SCF with time stepped smoothing : Real 2-FSK Signal



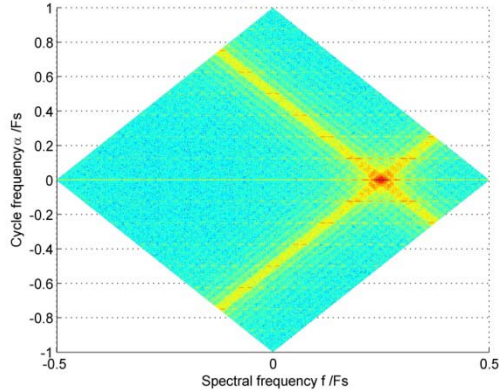
(a) FFT based SCF with time stepped smoothing : Real 2-FSK Signal

FFT based SCF with time stepped smoothing : Real BPSK Signal



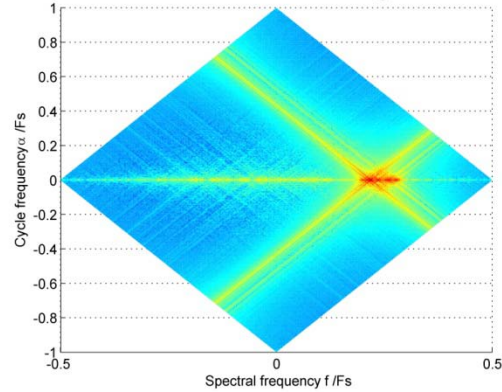
(b) FFT based SCF with time stepped smoothing : Real BPSK Signal

FFT based SCF with time stepped smoothing : Synthetic BPSK Signal



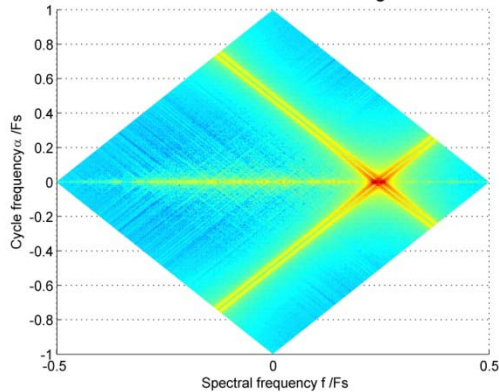
(c) FFT based SCF with time stepped smoothing : Synthetic BPSK Signal

FFT based SCF with time windowed smoothing : Real 2-FSK Signal



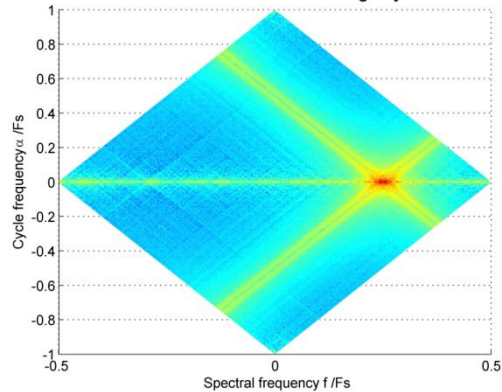
(d) FFT based SCF with time windowed smoothing : Real 2-FSK Signal

FFT based SCF with time windowed smoothing : Real BPSK Signal



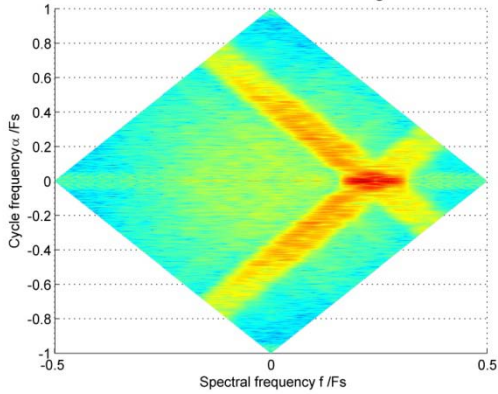
(e) FFT based SCF with time windowed smoothing : Real BPSK Signal

FFT based SCF with time windowed smoothing : Synthetic BPSK Signal



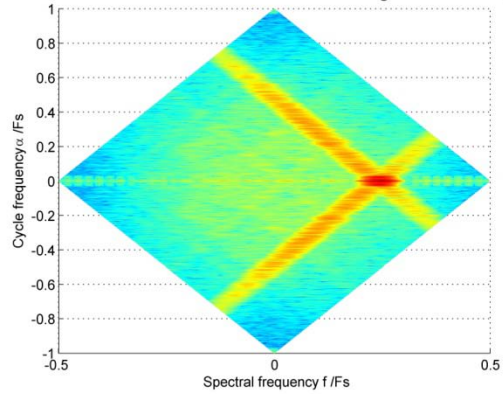
(f) FFT based SCF with time windowed smoothing : Synthetic BPSK Signal

CAF based SCF with time windowed smoothing : Real 2-FSK Signal



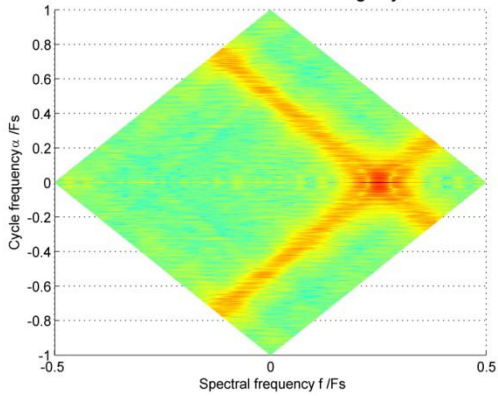
(g) CAF based SCF with time windowed smoothing : Real 2-FSK Signal

CAF based SCF with time windowed smoothing : Real BPSK Signal



(h) CAF based SCF with time windowed smoothing : Real BPSK Signal

CAF based SCF with time windowed smoothing : Synthetic BPSK Sign



(i) CAF based SCF with time windowed smoothing : Synthetic BPSK Signal

Figure 28. SCFs of real 2-FSK, BPSK, and synthetic BPSK using different computational approaches.

Bibliography

- [1] D. Cabric, S.M. Mishra, and R.W. Brodersen, "Implementation issues in spectrum sensing for cognitive radios," in *Signals, Systems and Computers, 2004. Conference Record of the Thirty-Eighth Asilomar Conference on*, 7-10 Nov. 2004, pp. pp. 772- 776.
- [2] J. Mitola, *Cognitive radio: Model-based competence for software radios*, 1999, Ph.D. dissertation, Dept. of Teleinformatics, KTH.
- [3] Yuan Qi, Wenbo Wang, Tao Peng, and Rongrong Qian, "Spectrum sensing combining time and frequency domain in multipath fading channels," in *Communications and Networking in China, 2008. ChinaCom*, 2008.
- [4] MaWenjie, Yang ShiMing, Ren Wu, Xue ZhengHui, and Li WeiMing, "Spectral correlation function in low SNR environment," in *Radio Science Conference*, 2004.
- [5] Antonio Napolitano, Luigi Paura William A. Gardner, "Cyclostationarity: Half a century of research," *Signal Processing*, vol. Volume 86, no. Issue 4, pp. Pages 639-697, April 2006.
- [6] W.A. Gardner and C.M. Spooner, "Signal interception: performance advantages of cyclic-feature detectors," *Communications, IEEE Transactions on*, vol. vol.40, no. no.1, pp. pp.149-159, Jan 1992.
- [7] Richard K. Martin, Ryan W. Thomas, and Zhiqiang Wu, "Using Spectral Correlation For Non-cooperative RSS-based Positioning," in *In Proceedings of IEEE SSP*, June 2011.
- [8] J. Goerlich et al., "Signal analysis using spectral correlation measurement," in *Instrumentation and Measurement Technology Conference, 1998. IMTC/98. Conference Proceedings. IEEE*, 18-21 May 1998, pp. pp.1313-1318.
- [9] Kyouwoong Kim et al., "Cyclostationary Approaches to Signal Detection and Classification in Cognitive Radio," in *New Frontiers in Dynamic Spectrum Access Networks, 2007. DySPAN 2007. 2nd IEEE International Symposium on*, 17-20 April 2007, pp. pp.212-215.

- [10] William A. Gardner, "The spectral correlation theory of cyclostationary time-series," *Signal Processing*, vol. Volume 11, no. Issue 1, pp. Pages 13-36, July 1986.
- [11] Kyou Woong Kim, Exploiting Cyclostationarity for Radio Environmental Awareness in Cognitive Radios, Dissertation.
- [12] Ryan W. Thomas and Richard K. Martin, "Closed Form Analysis of SCF Distribution for Signal Detection," *submitted to IEEE GLOBECOM*, 2011.
- [13] E. Like, V. Chakravarthy, R. Husnay, and Zhiqiang Wu, "Modulation Recognition in Multipath Fading Channels Using Cyclic Spectral Analysis," in *Global Telecommunications Conference, 2008. IEEE GLOBECOM 2008. IEEE*, Nov. 30 2008-Dec. 4 2008, pp. pp.1-6.
- [14] William A. Gardner, *Statistical Spectral Analysis – A Nonprobabilistic Theory*.: Prentice Hall, 1998.
- [15] W. Gardner, W. Brown, and Chih-Kang Chen, "Spectral Correlation of Modulated Signals: Part II--Digital Modulation," *Communications, IEEE Transactions on*, vol. vol.35, no. no.6, pp. pp. 595- 601, Jun 1987.
- [16] W.A. Gardner, "Spectral Correlation of Modulated Signals: Part I--Analog Modulation," *Communications, IEEE Transactions on*, vol. vol.35, no. no.6, pp. pp. 584- 594, Jun 1987.
- [17] H. Bolcskei, "Blind estimation of symbol timing and carrier frequency offset in wireless OFDM systems," *Communications, IEEE Transactions on* , vol. vol.49, no. no.6, pp. pp.988-999, Jun 2001.
- [18] A. Fehske, J. Gaeddert, and J.H. Reed, "A new approach to signal classification using spectral correlation and neural networks," in *New Frontiers in Dynamic Spectrum Access Networks, 2005. DySPAN 2005. 2005 First IEEE International Symposium on*, Nov. 2005, pp. pp.144-150,8-11.
- [19] D.Z. Vucic and M.M. Obradovic, "Cyclic spectral analysis of phase-incoherent FSK signal by matrix-based stochastic method," in *Telecommunications in Modern Satellite, Cable and Broadcasting Service, 2001. TELSIKS 2001. 5th International Conference on*, 2001, pp. 267-270.

- [20] Danijela Cabric Anant Sahai. (2005) Cyclostationary Feature Detection. [Online]. http://stewks.ece.stevens-tech.edu/NII-Research/RefLibrary/SKT-References/AS-web/BerkeleyWirelessCenter/Dyspan_2005_tutorial_part_2.pdf
- [21] D. Cabric, A. Tkachenko, and R.W. Brodersen, "Spectrum Sensing Measurements of Pilot, Energy, and Collaborative Detection," in *Military Communications Conference, 2006. MILCOM 2006. IEEE* , 23-25 Oct. 2006, pp. pp.1-7.
- [22] Niels Hoven , Rahul Tandra Anant Sahai, "Some Fundamental Limits on Cognitive Radio," in *Forty-second Allerton Conference on Communication, Control, and Computing*, 2004.
- [23] M.A.Ingram, Matched filter,
<http://www.ece.gatech.edu/research/labs/sarl/tutorials/ECE4606/14-MatchedFilter.pdf>.
- [24] Kimtho PO, and Jun-ichi TAKADA Sabita MAHARJAN. Energy Detector Prototype for Cognitive Radio System. [Online]. [http://www.ap.ide.titech.ac.jp/publications/Archive/IEICE_TRSR\(0707Sabita\).pdf](http://www.ap.ide.titech.ac.jp/publications/Archive/IEICE_TRSR(0707Sabita).pdf)
- [25] W.A. Gardner, "Signal interception: a unifying theoretical framework for feature detection," *Communications, IEEE Transactions on*, vol. vol.36, no. no.8, pp. pp.897-906, Aug 1988.
- [26] Hyoil Kim and Kang G. Shin, "In-band spectrum sensing in cognitive radio networks: energy detection or feature detection," in *Proceedings of the 14th ACM international conference on Mobile computing and networking*, 2008.
- [27] Tengyi Zhang, Guanding Yu, Chi Sun, "Performance of Cyclostationary Features Based Spectrum Sensing Method in A Multiple Antenna Cognitive Radio System," in *WCNC'09 Proceedings of the 2009 IEEE conference on Wireless Communications & Networking Conference*, IEEE Press Piscataway, NJ, USA , 2009, pp. 757-761.
- [28] John Grosspietsch, Gokhan Memik Zhuan Ye, "SPECTRUM SENSING USING CYCLOSTATIONARY SPECTRUM DENSITY FOR COGNITIVE RADIOS," in *Signal Processing Systems, 2007 IEEE Workshop on* ., Shanghai, China , Oct. 2007, pp. 1-6, 17-19.

- [29] Zhijin Zhao, Junna Shang Shiyu Xu, "Spectrum Sensing Based on Cyclostationarity," in *PEITS '08 Proceedings of the 2008 Workshop on Power Electronics and Intelligent Transportation System*, Washington, DC, USA, 2008, pp. 171-174.
- [30] S. Saunders, *Antennas and Propagation for Wireless Communication Systems*, 2nd ed.: John Wiley and Sons, Ltd, 2007.
- [31] Daniele Borio and Gérard Lachapelle Shashank Satyanarayana, Stationary, Cyclostationary and Nonstationary Analysis of GNSS Signal Propagation Channel, 2010,
http://plan.geomatics.ucalgary.ca/papers/iongnss10_student_shashank_20sep10.pdf.
- [32] S. Rappaport. Theodore, *Wireless Communications: Principles & Practice*. New Jersey: Prentice Hall, 1996.
- [33] John G. Proakis, *Digital communications*, 3rd ed. New York: McGraw-Hill, 1995.
- [34] A. Ghasemi and E.S. Sousa, "Collaborative spectrum sensing for opportunistic access in fading environments," in *New Frontiers in Dynamic Spectrum Access Networks, 2005. DySPAN 2005. 2005 First IEEE International Symposium on*, 8-11 Nov. 2005, pp. pp.131-136.
- [35] Zhe Dang, I. Howitt, R. McKinney, and J. Conrad, "First and second order statistics analysis for the RSS measurement in an indoor environment," in *IEEE SoutheastCon 2010 (SoutheastCon), Proceedings of the*, 18-21 March 2010, pp. pp.298-301.
- [36] P. D. Sutton, J. Lotze, K. E. Nolan, and L. E. Doyle, "Cyclostationary Signature Detection in Multipath Rayleigh Fading Environments," in *Cognitive Radio Oriented Wireless Networks and Communications, 2007. CrownCom 2007. 2nd International Conference on*, Aug. 2007, pp. pp.408-413.
- [37] Feng Ge and C.W. Bostian, "A Parallel Computing Based Spectrum Sensing Approach for Signal Detection under Conditions of Low SNR and Rayleigh Multipath Fading," in *New Frontiers in Dynamic Spectrum Access Networks, 2008. DySPAN 2008. 3rd IEEE Symposium on*, 14-17 Oct. 2008, pp. pp.1-10.

- [38] A. Tkachenko, A.D. Cabric, and R.W Brodersen, "Cyclostationary Feature Detector Experiments Using Reconfigurable BEE2," in *New Frontiers in Dynamic Spectrum Access Networks, 2007. DySPAN 2007. 2nd IEEE International Symposium on*, 17-20 April 2007, pp. pp.216-219.
- [39] David G. Messerschmitt, *How Digital Communication Works*, 1999,
<http://www.eecs.berkeley.edu/~messer/netappc/Supplements/20-digicom.pdf>,
University of California.
- [40] Inc. The MathWorks. FFT in Simulink. [Online].
<http://www.mathworks.com/help/toolbox/dspblks/ref/fft.html>
- [41] Muhammad Nabeel Mufti Adnan Aftab, *Spectrum Sensing Through Implementation of USRP2*, 2010, Master Thesis, School of Computing, Blekinge Institute of Technology, Sweden.
- [42] Ettus Research LLC, *USRP2, The Next Generation of Software Radio Systems*,
http://www.ettus.com/downloads/ettus_ds_usrp2_v5.pdf.
- [43] V. Erceg et al., ""An empirically based path loss model for wireless channels in suburban environments,"" *Selected Areas in Communications, IEEE Journal on*, vol. vol.17.
- [44] Michael A. Crane and Donald L. Iglehart, "Simulating Stable Stochastic Systems: III. Regenerative Processes and Discrete-Event Simulations," *Operations Research*, vol. Vol. 23 , no. Issue 1, pp. p33-45, Jan/Feb 1975.
- [45] NIST/SEMATECH. (2003, May) NIST/SEMATECH e-Handbook of Statistical Methods. [Online].
<http://www.itl.nist.gov/div898/handbook/eda/section3/normprp3.htm>

Vita

Captain Mujun Song graduated from Sin-do high school in Busan, Korea. He received his Bachelors degree of engineer in Electrical Engineering from Korea Military Academy in 2005. After graduation, he was commissioned in the 62th signal battalion as a communication officer. In December 2006, he was deployed to Arbil, Iraq as a communication officer in Zaytun Division. Before attending the Air Force Institute of Technology (AFIT) in July 2007, he was assigned to the United Nations Command Security Battalion - Joint Security Area (UNCSB-JSA) as a Korean communication officer. His next assignment is the Officer Advanced Course (OAC) for communication officers.

REPORT DOCUMENTATION PAGE

Form Approved
OMB No. 074-0188

The public reporting burden for this collection of information is estimated to average 1 hour per response, including the time for reviewing instructions, searching existing data sources, gathering and maintaining the data needed, and completing and reviewing the collection of information. Send comments regarding this burden estimate or any other aspect of the collection of information, including suggestions for reducing this burden to Department of Defense, Washington Headquarters Services, Directorate for Information Operations and Reports (0704-0188), 1215 Jefferson Davis Highway, Suite 1204, Arlington, VA 22202-4302. Respondents should be aware that notwithstanding any other provision of law, no person shall be subject to a penalty for failing to comply with a collection of information if it does not display a currently valid OMB control number.

PLEASE DO NOT RETURN YOUR FORM TO THE ABOVE ADDRESS.

1. REPORT DATE (DD-MM-YYYY) 16-06-2011		2. REPORT TYPE Master's Thesis		3. DATES COVERED (From – To) September 2009 – June 2011		
4. TITLE AND SUBTITLE Characterizing Cyclostationary Features of Digital Modulated Signals with Empirical Measurements using Spectral Correlation Function				5a. CONTRACT NUMBER		
				5b. GRANT NUMBER		
				5c. PROGRAM ELEMENT NUMBER		
				5d. PROJECT NUMBER 11G171		
				5e. TASK NUMBER		
				5f. WORK UNIT NUMBER		
7. PERFORMING ORGANIZATION NAMES(S) AND ADDRESS(S) Air Force Institute of Technology Graduate School of Engineering and Management (AFIT/EN) 2950 Hobson Way, Building 640 WPAFB OH 45433-8865				8. PERFORMING ORGANIZATION REPORT NUMBER AFIT/GCE/ENG/11-09		
9. SPONSORING/MONITORING AGENCY NAME(S) AND ADDRESS(ES) Steve Brooks (BCSI) Deputy for AT/FP Technologies SEA SHIELD FNC Office of Naval Research 875 North Randolph Street, Suite 1109 Arlington, VA 22203-1995 steven.brooks1.ctr@navy.mil 703-588-2397				10. SPONSOR/MONITOR'S ACRONYM(S) ONR		
12. DISTRIBUTION/AVAILABILITY STATEMENT APPROVED FOR PUBLIC RELEASE; DISTRIBUTION UNLIMITED.				11. SPONSOR/MONITOR'S REPORT NUMBER(S)		
13. SUPPLEMENTARY NOTES This material is declared a work of the U.S. Government and is not subject to copyright protection in the United States						
14. ABSTRACT Signal detection is widely used in many applications. Some examples include Cognitive Radio (CR) and military intelligence. CRs use signal detection to sense spectral occupancy. Without guaranteed signal detection, a CR cannot reliably perform its role. Similarly, signal detection is the first step for garnering an opponent's information. Wireless signal detection can be performed using many different techniques. Some of the most popular include matched filters, energy detectors (which use measurements such as the Power Spectral Density (PSD) of the signal), and Cyclostationary Feature Detectors (CFD). Among these techniques, CFD can be viewed as a compromise technique, in that it theoretically has better low Signal-to-Noise Ratio (SNR) detection performance than energy detectors and less strict requirements than matched filters. CFD uses the cyclostationarity of a signal to detect its presence. Signals that have cyclostationarity exhibit correlations between widely separated spectral components. Functions that describe this cyclostationarity include the Spectral Correlation Function (SCF). One advantage of cyclostationary approaches such as these is that Additive White Gaussian Noise (AWGN) is cancelled in these functions. This characteristic makes SCF outperform PSD under low SNR environments. However, whereas PSD has been well investigated through empirical experiments throughout many researches, SCF features under real world noise have not been investigated with empirical experiments. In this effort, firstly, the SCF features of modulated signals under real world channel noise are identified and characterized using the concept of path loss. Secondly, outperformance of SCF under low SNR environment with real world signals is verified with real world signals and noise. In addition, dependence between finite time parameter of SCF calculation, which is observation time, and SCF feature statistics are identified with real world signals. Lastly, a reason for discrepancy of SCF performance between analytic / simulation based approach and real world experimental approach is suggested.						
15. SUBJECT TERMS						
16. SECURITY CLASSIFICATION OF:			17. LIMITATION OF ABSTRACT UU	18. NUMBER OF PAGES 107	19a. NAME OF RESPONSIBLE PERSON Ryan W. Thomas, Major, USAF	
REPORT U	ABSTRACT U	c. THIS PAGE U			19b. TELEPHONE NUMBER (Include area code) (937) 255-3636 4613 ryan.thomas@afit.edu	